HELLENIC REPUBLIC
National and Kapodistrian University of Athens
School of Science
Department of Physics

SYK Model and Quantum Chaos

Stavros Efthymiou
Nuclear and Particle Physics Section

A thesis submitted in partial fulfillment for the degree of B.Sc. in Physics

Supervisor:
Aris L. Moustakas
Division of Applied Physics

Athens, 2017

"More is different."

P. W. Anderson

Abstract

In this work we study the Sachdev-Ye model for random quantum magnets and attempt an introduction to a modern reintroduction of it, proposed by A. Kitaev as an attempt to connect it with gravitational problems. The introduction focuses on the chaotic characteristics of the SYK model.

Firstly we present the solution of Sachdev-Ye model in detail and we find the analytic expressions for the Green's function in appropriate limits of total spins, low frequencies and zero temperature. From physics perspective, the main result is the magnetic susceptibility, which diverges as $\chi \sim \ln T$, slower than the famous Curie law. This is a characteristic of the exotic behavior of spin liquids, because of the strong quantum fluctuations. This spin liquid phase is the phenomenon that the model tries to describe. This phase exists in both fermionic and bosonic representation of spins under appropriate conditions. However, there is a major difference as in the bosonic representation there is a transition to a spin glass phase even in zero temperature. Finally, using symmetry arguments we can extend the analytic solutions for the Green's function in non-zero temperatures. This result is useful for the analysis in the following chapters.

In the following chapters we study the modern edition of the model and mainly its chaotic characteristics. These characteristics are crucial in the connection between the model and gravitational problems. Quantitatively they can be found by studying the out-of-time-ordered correlator. In chapter 3 we attempt to qualitatively introduce this quantity in analogy with classical chaos and give a definition for the quantum butterfly effect. Through an example with a simple qubit system we also show how chaotic many body systems scramble information. This connection is of great interest in the context of black hole physics.

In chapter 4 we present the calculation of the out-of-time-ordered correlator for the complex SYK model in detail, using the Green's function we found for the Sachdev-Ye model. The goal is the calculation of the corresponding Lyapunov exponent which is done analytically but also corroborated arithmetically. We find the value $\lambda_{\mathrm{L}} = 2\pi k_B T/\hbar$ which is proven to be the maximum possible value for a quantum many body system. This is an indication that the model has a gravity dual.

Acknowledgements

This work was conducted during 2016-17 my final year of studies in the Physics Department of the University of Athens. I would like to thank my supervisor Prof. A. Moustakas for proposing a very interesting and cutting-edge subject, which I was not aware of before starting this work. Moreover, our discussions were enlightening and helped me expand my knowledge in the field of condensed matter theory, even outside the scope of this work.

I would also like to note that there are no new ideas in this work, as all the concepts presented are based on older publications. Chapter 2 is mostly based in the work of S. Sachdev and J. Ye in [2] and SYK model was proposed in [7][8] by A. Kitaev and was studied in more detail in [9] by D. Stanford and J. Maldacena. A great part of the technical calculations was included in [10] by S. Banerjee and E. Altman and this was very helpful in understanding the concepts. Other publications were used as well which are included in the bibliography.

My goal was to gather information from different sources and present this modern subject of theoretical physics in a simple way, ideally understandable by undergraduate students. At the same time I had the chance to become familiar with problems that are subject of currently ongoing research. I hope to have the chance to work on these problems more thoroughly in the future.

Contents

Chapter 1

Introduction

1.1 Quantum Spin Liquids

Fermi liquid theory, proposed by L. Landau, describes most metallic solids. In contrast with the famous Fermi gas, this theory describes interacting fermions. However, interactions are enabled slowly (adiabatically) and the description is possible by changing some parameters (for example the mass changes because of the interaction to a new effective mass). Hence, the description is technically close to this of Fermi gas theory.

Although Fermi liquid gives correct results for most metals even in low temperatures, it fails to describe some exotic behaviors of matter, like superconductivity or superfluidity[1]. For the description of such phenomena we have to study strongly interacting fermionic systems. An example of a phase that emerges in such systems, which exists in the Sachdev-Ye (SY) model that we study in the following chapters, is the spin liquid phase. The main phenomenon taking place in this phase is the destruction of classical magnetic ordering because of strong quantum fluctuations.

In order to understand better these terms, it is better to start with the famous Heisenberg model for interactions between neighboring spins. The corresponding Hamiltonian is:

$$\hat{H} = -J \sum_{\langle ij \rangle} \hat{\mathbf{S}}_i \cdot \hat{\mathbf{S}}_j \tag{1.1}$$

[1]Another parameter that is crucial for the validity of Fermi liquid theory is space dimension. For example, in one dimension this theory is not valid and it is replaced by Luttinger liquids.

Here $\hat{\mathbf{S}}_i$ are spin operators that follow SU(2) algebra, in contrast to the Ising model which uses a classical image of spins. The $\langle ij \rangle$ symbol denotes sum to nearest neighbors and the lattice shape and dimension is arbitrary.

We also note that in the model 1.1 particles (for example electrons) are frozen in specific lattice sites and the only interaction between them is caused by their spin. There is not Coulomb interaction. This simplification is made because we would like to focus on the results that are caused by magnetic interactions. However, it might indeed be valid in a real system, where the electrons are localized in specific sites of the atoms.

It is known from Statistical Physics that equilibrium in many body systems is described by the canonical (Boltzmann) ensemble where the probability of a microstate of energy E is $P \sim e^{-\beta E}$. This means that microstates of small energy are preferred, or better, there is higher probability for the system to be in one of those.

Applying this observation in 1.1 we find that for $J > 0$, microstates in which nearest neighbors have aligned spins are preferred. In such a state we have order, namely the direction of the thermal expectation value $\left\langle \hat{\mathbf{S}}_i \right\rangle$ is specified. Experimentally this order is identified by the ferromagnetic behavior of the solid.

The case where $J < 0$ is more complex. Then we need anti-aligned spins in order to minimize the energy. It is not always possible to build such a state uniquely. For example, in a square lattice we may alternate the spin direction between up and down. This way every nearest neighbor bond contributes $-J$ which is its minimum contribution.

The difficulty appears in an example proposed by P. Anderson [11], where the lattice is triangular. It is apparent that in such a system it is impossible for both bonds in a triangle to contribute with their minimum energy. We call this phenomenon frustration because the two competitive interactions cannot be satisfied at the same time. There are many different microstates with the same energy (for example six in the triangle), which have the same probability of appearance. We can imagine two similar systems which, because of frustration, end up to different equilibriums. The result is the destruction of the magnetic order that ferromagnetic materials have.

Finally, we note that frustration that appears in the triangular lattice example is not only theoretical, but also real materials have been found that show spin liquid behavior. A common lattice with a triangular form is Kagome (Trihexagonal). The mineral Herbertsmithite, which has this structure, seems to have some spin liquid characteristics. [12]

1.2 Sachdev-Ye model

In the main body of this work and mostly in Chapter 2 we will analyze the model proposed by S. Sachdev and J. Ye in [2]. The corresponding Hamiltonian is:

$$\mathcal{H} = \frac{1}{\sqrt{NM}} \sum_{i>j} J_{ij} \hat{\mathbf{S}}_i \cdot \hat{\mathbf{S}}_j \tag{1.2}$$

Despite the similarities between 1.2 and the already famous Heisenberg model of 1.1, there are important differences that lead to completely different behavior of the system. For example, spin operators in the SY model follow SU(M) algebra and the problem can be analytically solved only in the limit $M \to +\infty$. We have not found any published analytic solution for $M = 2$.

Moreover, a main difference that simplifies the SY model is that the sum is extended to all sites, not only nearest neighbors, as in the Heisenberg model. This approximation is common in the context of mean field theory and here it is also crucial in order to obtain analytic solutions. Finally, J_{ij} coefficients, which measure how strong the interactions are, follow a normal distribution with zero mean and variance J^2.

The randomness of J_{ij} combined with the mean field approximation seem to make the model unrealistic. For example, two neighboring sites might interact weakly, while two other, which are located far from each other, might interact strongly. A possible solution of this is to think that in mean field theories, an exclusive pair interaction is not important, as the motion of the particle is affected by the total effective interaction that it feels, which is a sum of all pair interactions. Here we have infinitely many particles and we expect that the final sum will be realistic.

It is apparent that in the mean field approximation the results are independent of lattice structure. Since the sum is not restricted to nearest neighbors, we do not expect frustration for the reasons we had it in the triangular lattice. Sachdev and Ye were after a model that is analytically solvable and exhibits a spin liquid ground state, where we have strong quantum fluctuations. Either the randomness in J_{ij} or the limit $M \to +\infty$ seem to be crucial in this.

This was not the first time that random J_{ij} were used in such problems. This technique was already applied in classical problems of spin glasses (the term is related to the disorder in the positions of the molecules in common glasses). In a way, SY Hamiltonian is like a quantum generalization of the Sherrington-Kirkpatrick model for classical spin glasses [13],

which is also a mean field model. In fact, it is noted in [2] and further studied in [3] and [4], that for specific values of the parameters and temperature, SY model exhibits a quantum spin glass ground state.

In any case, there are realistic reasons for the randomness of interactions. For example, defects exist in every material and we do not know their exact distributions so we describe them using probability distributions. We expect that such phenomena exist in low temperatures where thermal randomness is weaker (compared to higher temperatures).

Here we are mostly interested in the spin liquid phase rather than the spin glass. The major difference is in the source of the disorder, as in the former this is mainly the quantum fluctuations. It is not apparent whether the disorder in the SY model is caused by the randomness of J_{ij} or in the unrealistic limit $M \to +\infty$. In [5] the SY model is solved arithmetically for realistic SU(2) spins using quantum Monte Carlo methods. Although the results for the spin glass phase seem to agree with the analytical solutions in the $M \to +\infty$ approximation, this is not valid for the spin liquid phase. A possible explanation is that the limit $M \to +\infty$ causes high degeneracy in the ground state and this serves as the source for strong quantum fluctuations [4].

1.3 Kitaev's Proposal

Several years after the introduction of the SY model for random quantum magnets, A. Kitaev proposed the SYK Hamiltonian:

$$H = \frac{1}{4!} \sum_{jklm} J_{jklm} \chi_j \chi_k \chi_l \chi_m \tag{1.3}$$

Coefficients J_{jklm} are still random numbers, however the operators represent Majorana fermions and are Hermitian (real). In the old SY model spins are usually represented in complex fermionic operators (Chapter 2).

The new model was not introduced to describe a state of matter, but as a simple model of holography. The term is used in quantum gravity theories where it is believed that the description of a system can be done in its boundary, which has one less dimension that the real system (in analogy with common holograms which are 3-dimensional schemes in a 2-dimensional space).

More specifically the analogy that comes from SYK is in the context of AdS_2/CFT_1 correspondence. In general, with AdS/CFT [14] we mean an analogy between Anti-de-Sitter space, used in quantum gravity theories and a conformal field theory. Such correspondence corroborates the holographic principle, as the AdS space of d-dimensions corresponds to a CFT in $d-1$ dimensions.

Quantum fluctuations are important in such a theory, and hence the spin liquid phase of SY shall be used. In Kitaev's model we can destroy the spin glass phase by taking a single limit $N \to +\infty$. In contrast, in the old SY, as we will see, we need to use the fermionic representation of spins and take two limits $N, M \to +\infty$. [6]

As we will find in the following chapters, the resulting Schwinger-Dyson equations for both SY and SYK have conformal symmetry at low frequencies (infrared). This symmetry is one of the reasons Kitaev proposed this model as a CFT for holography. The CFT is 1-dimensional, we have only time (recall that sites are frozen in space so we do not have spatial dimensions). The conformal symmetry breaks in higher frequencies (ultraviolet) and this mechanism has similarities with gravity near extremal black holes, where the space is AdS_2 (2-dimensional). [9]

Apart from the conformal symmetry argument, another fact that links SYK with gravitational problems is chaos, which mathematically appears when studying the out-of-time-ordered correlators (OTOC). In [15] a way to define Lyapunov exponent for a quantum many body system is given. Using this the authors prove that exists a maximum value that this exponent can have. It is conjectured that systems that saturate this bound have a gravity dual. SYK satisfies this, namely it is maximally chaotic.

Because of these arguments the model was subject of extensive research work during the last two years. The fact that it is one of the few analytically solvable models (in the limit $N \to +\infty$ the non-crossing approximation is valid and we can sum the diagrams) makes the model more interesting. The solvability is impressive if we think that it is a chaotic (in fact maximally chaotic) system! [16] Even in classical mechanics, chaotic systems are not solvable.

1.4 Structure of this thesis

In the second chapter we will work on the Sachdev-Ye model. More specifically we will follow [2] giving more details in some of the calculations. The main result, from the

experimentalist's perspective, is related to the magnetic susceptibility which diverges logarithmically at low temperatures. We will also use the conformal and gauge symmetry of the equations to extend Green's functions to non-zero temperature. These symmetries were not included in the first publication [2] but were noted afterwards [4][8] and the results are important for the chaos calculations in Chapter 4.

In the third chapter we will pursue to give the meaning of the OTO correlators as a measure of quantum chaos, or better, the scrambling of information. There are many questions about this subject and relevant research is taking place currently. Therefore, the presentation is mostly qualitatively and not mathematically rigorous. Generally, this quantum generalization of chaos is different from others (for example in systems with a classical analogue [17]), however it is useful in the gravity correspondence.

In the fourth chapter we will come back to the SY model and a similar one, which is a complex generalization of SYK. We will calculate the OTO correlators introduced before using the results of Chapter 2. The resulting Lyapunov exponent will be the bound proposed in [15].

Someone might say that the subjects of the following three chapters are not entirely relevant. This is generally true, as half of the work is on a quantum many body system which exhibits some exotic magnetic properties while the rest is on an abstract generalization of chaos in relation to black hole physics. However, we believe that the interesting point of this topic is exactly the fact that relates these, seemingly unrelated, concepts.

The connection is useful for two reasons: There are benefits from the theoretical physics perspective, as mathematically connecting two theories enables us to transfer problems from one to another and use tools from one on problems of the other. Till now AdS/CFT correspondence was used to transform difficult CFT problems to easy gravitational problems, but SYK shows that the inverse is also possible [18]. There are also benefits from the experimentalist's point of view. Systems that we cannot access, like black holes, are corresponded to condensed matter physics systems, which are accessible for experimental study. [19]

Chapter 2

Sachdev-Ye model for Random Quantum Magnets

We will first analyze the Sachdev-Ye model introduced in [2]. As we stated in the introduction the main purpose for this proposal was to present a solvable model that has a spin liquid phase in its ground state. The Hamiltonian is:

$$\mathcal{H} = \frac{1}{\sqrt{NM}} \sum_{i,j=1}^{N} J_{ij} \hat{\mathbf{S}}_i \cdot \hat{\mathbf{S}}_j \tag{2.1}$$

where $\hat{\mathbf{S}}_i$ are operators that obey the SU(2) algebra and N is the total number of sites. The problem becomes analytically solvable in the limits $N, M \to +\infty$.

In the original model, the coefficients J_{ij} are independent random variables that follow a normal distribution with zero average and variance $\overline{J_{ij}^2} = J^2$. According to [7] the exact distribution does not really affects the system's behavior. The reason is that, since we have a mean-field-like model, the total force that each site feels comes from a superposition of all possible interactions. Therefore, we can think of this total interaction as a sum of many (infinitely when $N \to +\infty$) random variables and invoke the central limit theorem to argue that the effective distribution will be normal, independently of the starting distributions. In any case, J_{ij} must be independent and identically distributed random variables.

We will present the results of the original work [2] with more detailed calculations. The main result is the local susceptibility at low temperatures which diverges logarithmically,

much slower than the typical $\sim 1/T$ of Curie law [4]. This result is characteristic of the disorder that is caused by quantum fluctuations in the spin liquid state.

Moreover, the work of this chapter is essential to the calculation of the chaos exponent in the last chapter. Specifically the low frequency Green's functions that were originally calculated in [2]) at zero temperature can be extended, using the symmetries of Schwinger-Dyson equations, to non-zero temperature. These functions constitute the kernel in the OTO correlator integral equation in the chaos region.

2.1 Coherent state path integral

The SY model of Eq 2.1 can only be solved in the limit $N \to \infty$. In this limit we can establish a mean-field theory, by expressing the partition function as a coherent state path integral and applying the replica method. The advantage of this method is that the interaction between different spins is transformed into interaction between replicas of a single spin.

We start by using the canonical fermion operators $c_{i\alpha}$ which obey the anticommutation relations:

$$\{c_{i\alpha}, c_{j\beta}\} = 0 \quad , \quad \{c_{i\alpha}, c^\dagger_{j\beta}\} = \delta_{ij}\delta_{\alpha\beta} \tag{2.2}$$

and the Hamiltonian 2.1 takes the following form:

$$\mathcal{H} = \frac{1}{\sqrt{NM}} \sum_{i,j=1}^{N} \sum_{\alpha,\beta=1}^{M} J_{ij} c^\dagger_{i\alpha} c_{i\beta} c^\dagger_{j\beta} c_{j\alpha} \tag{2.3}$$

with the fermion number constraint:

$$\sum_{\alpha=1}^{M} c^\dagger_{i\alpha} c_{i\alpha} = MQ \tag{2.4}$$

on every site i. This form of the Hamiltonian is given in [6]. The SYK model is a simpler realization of this form where the fermions are substituted by Majorana fermions and a single limit $N \to \infty$ is required.

In order to write 2.3 as a path integral we make use of the coherent states $|\psi\rangle$ of the fermionic operators, for which:

$$c_{i\alpha} |\psi\rangle = \psi_{i\alpha} |\psi\rangle \tag{2.5}$$

These states satisfy the completeness relation:

$$\int \exp\left(-\sum_{ia} \bar{\psi}_{i\alpha}\psi_{i\alpha}\right) |\psi\rangle \langle\psi| \, d(\bar{\psi},\psi) = \mathbf{I} \tag{2.6}$$

Thus the partition function can be written as:

$$\mathcal{Z} = \int \exp\left(-\sum_{ia} \bar{\psi}_{i\alpha}\psi_{i\alpha}\right) \langle\psi| \, e^{-\beta\mathcal{H}} \, |\psi\rangle \, d(\bar{\psi},\psi) =$$

$$= \int \exp\left[-\int_0^\beta \left(\bar{\psi}(\tau)\left(\partial_\tau - \mu\right)\psi(\tau) + H(\bar{\psi},\psi)\right) d\tau\right] D(\bar{\psi},\psi)$$

where we used the completeness relation 2.6 to partition the imaginary time interval $[0,\beta]$. The chemical potential μ was introduced because of the constraint 2.4.

The important part of the integral is the one that corresponds to the Hamiltonian H, so we will focus out attention on this. Using 2.5 and its Hermitian conjugate we find:

$$H(\bar{\psi},\psi) \equiv \langle\psi| \, \mathcal{H} \, |\psi\rangle = \frac{1}{\sqrt{NM}} \sum_{i,j=1}^{N} \sum_{\alpha,\beta=1}^{M} J_{ij}\bar{\psi}_{i\alpha}\psi_{i\beta}\bar{\psi}_{j\beta}\psi_{j\alpha}$$

Hence, the partition function can be expressed as the path integral:

$$\mathcal{Z} = \int \exp\left[-\frac{1}{\sqrt{NM}} \sum_{i,j=1}^{N} J_{ij} \int_0^\beta \mathbf{S}_i(\tau)\cdot\mathbf{S}_j(\tau) d\tau\right] D\mathbf{S} \tag{2.7}$$

where the measure $D\mathbf{S}$ is a product of the measures for all sites: $D\mathbf{S} = D\mathbf{S}_1 ... D\mathbf{S}_N$. The next step is to introduce n replicas of the system and average over the J_{ij} distribution, following [20]:

$$\overline{\mathcal{Z}^n} = \int D\mathbf{S} \prod_{a=1}^{n} \prod_{i,j=1}^{N} \int_{-\infty}^{\infty} dJ_{ij}^a P(J_{ij}^a) \exp\left[-\frac{1}{\sqrt{NM}} J_{ij}^a \int_0^\beta \mathbf{S}_i^a(\tau)\cdot\mathbf{S}_j^a(\tau) d\tau\right]$$

where

$$P(J_{ij}) = \frac{1}{\sqrt{2\pi}J} e^{-J_{ij}^2/(2J^2)} \tag{2.8}$$

The J_{ij}^a integral is Gaussian and its evaluation is straightforward:

$$\overline{\mathcal{Z}^n} = \int \exp\left[\frac{J^2}{2NM} \sum_{a,b=1}^{n} \sum_{i,j=1}^{N} \int_0^\beta \int_0^\beta \left[\mathbf{S}_i^a(\tau)\cdot\mathbf{S}_j^a(\tau)\right]\left[\mathbf{S}_i^b(\tau')\cdot\mathbf{S}_j^b(\tau')\right] d\tau d\tau'\right] D\mathbf{S} \tag{2.9}$$

In order to decouple the spins of different sites we apply a Hubbard-Stratonovich transformation. This can be thought as applying a generalization of the formula $\int e^{-ax^2+bx} = e^{b^2/(4a)}$ for path integrals to express the exponential of 2.9 as a path integral of another function Q. Using the summation convention (repeated indeces are summed) the partition function is:

$$\overline{\mathcal{Z}^n} = \int e^{-N\mathcal{F}[\mathbf{Q}]} D\mathbf{Q} \tag{2.10}$$

where

$$\mathcal{F}[\mathbf{Q}] = \frac{MJ^2}{4} \iint_0^\beta \left(Q^{ab}_{\mu\nu}(\tau,\tau')\right)^2 d\tau d\tau' - \ln \int e^{\mathcal{L}[\mathbf{S}]} D\mathbf{S} \tag{2.11}$$

and

$$\mathcal{L}[\mathbf{S}] = \frac{J^2}{2M} \iint_0^\beta Q^{ab}_{\mu\nu}(\tau,\tau') S^a_{i\mu}(\tau) S^b_{i\nu}(\tau') d\tau d\tau' \tag{2.12}$$

In the limit $N \to \infty$ we can use the saddle point method to evaluate the integral in 2.10. The saddle point of the functional $\mathcal{F}$ can be found by eliminating the first order of $\delta\mathbf{Q}$ in the difference $\delta\mathcal{F} = \mathcal{F}[\mathbf{Q}+\delta\mathbf{Q}] - \mathcal{F}[\mathbf{Q}]$. This gives:

$$\begin{cases} \int e^{\mathcal{L}} \delta\mathcal{L} D\mathbf{S} = \dfrac{MJ^2}{2} \displaystyle\int e^{\mathcal{L}} D\mathbf{S} \iint_0^\beta Q^{ab}_{\mu\nu}\, \delta Q^{ab}_{\mu\nu} d\tau d\tau' \\ \delta\mathcal{L} = \dfrac{J^2}{2M} \displaystyle\iint_0^\beta \delta Q^{ab}_{\mu\nu} S^a_{i\mu} S^b_{i\nu} d\tau d\tau' \end{cases}$$

which reduces to:

$$\iint_0^\beta \delta Q^{ab}_{\mu\nu} \left[\int S^a_{i\mu}(\tau) S^b_{i\nu}(\tau') e^{\mathcal{L}} D\mathbf{S} - M^2 Q^{ab}_{\mu\nu} \int e^{\mathcal{L}} D\mathbf{S} \right] = 0 \Rightarrow$$

$$\Rightarrow Q^{ab}_{\mu\nu}(\tau,\tau') = \frac{1}{M^2} \left\langle S^a_{i\mu}(\tau) S^b_{i\nu}(\tau') \right\rangle \tag{2.13}$$

where the symbol $\langle \bullet \rangle$ is defined as:

$$\langle \bullet \rangle = \frac{\int \bullet\, e^{\mathcal{L}} D\mathbf{S}}{\int e^{\mathcal{L}} D\mathbf{S}} \tag{2.14}$$

Equation 2.13 gives the saddle point of the functional $\mathcal{F}$ which we can use in 2.10 to evaluate the partition function of a single-site:

$$\overline{\mathcal{Z}^n} \sim e^{-\mathcal{F}[\mathbf{Q}]} = \int e^{\mathcal{L}[\mathbf{S}]} D\mathbf{S} \tag{2.15}$$

where $\mathcal{L}$ is given by 2.12. The symbol $\sim$ is used in 2.15 because we may have neglected

some multiplicative constants. We argue that these constants do not have physical significance in the $N \to \infty$ limit.

We note that using the replica method we decoupled the sites and as a result the total partition function is a product of the single-sites of 2.15. Moreover, due to this expression of the partition function, the symbol we defined in 2.14 is actually the thermal average over different configurations of spins.

The partition function of 2.15 is linked with measurable quantities and must be invariant under rotations of the reference frame. Consequently, it is reasonable to assume that the same is valid for the saddle point of 2.13, meaning that we can eliminate the indices μ, ν which are related with the different 'spatial' components[1] of spin. To be more specific, the average vanishes for $\mu \neq \nu$ and for the case $\mu = \nu$ we can write an inner product:

$$Q^{ab}(\tau - \tau') = \frac{1}{M^2} \left\langle \mathbf{S}^a(\tau) \cdot \mathbf{S}^b(\tau') \right\rangle \tag{2.16}$$

At a similar manner 2.12 gives:

$$\mathcal{L}[\mathbf{S}] = \frac{J^2}{2M} \int_0^\beta \int_0^\beta Q^{ab}(\tau - \tau') \mathbf{S}^a(\tau) \cdot \mathbf{S}^b(\tau') d\tau d\tau' \tag{2.17}$$

Another remark can be made on the replica indices. As the average of 2.16 can be interpreted as a correlation between different replicas it could be expected to vanish for $a \neq b$. However, this is not valid in the spin-glass phase which exists because of the randomness of the interactions (the J_{ij} in the Hamiltonian 2.1). On the other hand, in the spin-fluid phase, the quantum fluctuations are the dominant reason for the disorder and all the correlations are replica diagonal.

If we consider the replica diagonal terms of 2.16 we get a correlation between spins of a single site at different times. This relates Q with a experimentally measurable quantity, the magnetic susceptibility $\chi(\tau) = Q^{aa}(\tau)$. The main goal of [2] and a large part of this chapter is to find an analytic expression for this quantity. This is done by treating the interaction defined by 2.17 as a perturbation to the free-particle Lagrangian.

[1] If we recall how we proceeded from 2.9 to 2.12, we will see that the μ, ν indeces were used to write the inner product $\mathbf{S}_i \cdot \mathbf{S}_j = S_{i\mu} S_{j\mu}$

2.2 Total spin limits

The limit $N \to \infty$ helped us to express the problem in the mean-field approximation. In order to make the problem analytically solvable, even in this approximation, we also have to take specific limits for the spin order M or the maximum spin S.

The limit $N \to \infty$ can easily be explained, as it corresponds to a system with a great number of sites. After all, this is always the case in statistical physics. On the other hand, the real spin systems are SU(2), that is $M = 2$, and for electrons $S = 1/2$, so it is not straightforward how this is consistent with the limits $M, S \to \infty$. By taking these limits we expect to find results that are approximately valid in the physical case, rather than solving the problem exactly.

The limit $S \to \infty$ with M fixed is the easiest to understand. The quantum properties of spins stem from the non-commutativity of the corresponding operators: $[\hat{S}_i, \hat{S}_j] = i\epsilon_{ijk}\hat{S}_k$. In the limit $S \to \infty$ we can write:

$$[S\hat{\sigma}_i, S\hat{\sigma}_j] = i\epsilon_{ijk}S\hat{\sigma}_k \Rightarrow [\hat{\sigma}_i, \hat{\sigma}_j] = i\epsilon_{ijk}\frac{\hat{\sigma}_k}{S} \to 0$$

which can be thought as if the spins lose their quantum property of non-commutativity and act like classical quantities. Consequently, in the limit $S \to \infty$ the systems behaves semi-classicaly and its ground state is a classical spin-glass. We do not expect to find the quantum spin-fluid phase in this limit.

The second possibility is the limit $M \to \infty$ with S fixed. This cannot be explained intuitivelly as in the previous case. We examine this limit using the fermionic representation for the spins, $S_{\mu\nu} = c^\dagger_\mu c_\nu$ with the constraint $\sum_\mu f^\dagger_\mu f_\mu = Mq_0$, with $0 \leq q_0 \leq 1$, as in 2.4. We find that the quantum fluctuations are very strong in this limit, resulting in a ground state that is always a spin-liquid.

Finally, the interesting case is the limit $M, S \to \infty$, with their ratio $\kappa = 2S/M$ fixed. This limit is achieved by the Schwinger's boson representation: $S_{\mu\nu} = b^\dagger_\mu b_\nu$ with $\sum_\mu b^\dagger_\mu b_\mu = 2S$. In this case both the spin-fluid and the spin-glass ground states exist, depending on the value of κ. Note that small κ roughly means small spin and strong quantum fluctuations, characteristic of the spin-liquid. As κ increases we expect a transition to the spin-glass phase.

2.3 Schwinger-Dyson equations

The properties of the system in each phase can be understood quantitatively by computing the Green's functions. The functions that are interesting to our problems are related to each of the two representations which we presented in the previous section:

$$G_B^{ab}(\tau) = \frac{1}{M}\left\langle T b_\mu^a(\tau) b_\mu^{b\dagger}(0)\right\rangle \quad , \quad G_F^{ab}(\tau) = \frac{1}{M}\left\langle T f_\mu^a(\tau) f_\mu^{b\dagger}(0)\right\rangle \tag{2.18}$$

where thermal averages are taken in respect to the full Hamiltonian, that is the free particle and the interaction expressed by the functional 2.17. The time ordering symbol T means that the operators are ordered according to history:

$$\langle T A(\tau)B(\tau')\rangle = \Theta(\tau-\tau')A(\tau)B(\tau') \pm \Theta(\tau-\tau')A(\tau)B(\tau') \tag{2.19}$$

where Θ denotes Heaviside's step function. The middle sign is $+$ for bosons and $-$ for fermions and it is a result of the commutation (anticommutation) relations of the bosonic (fermionic) operators.

Generally b and f in 2.18 can be thought as operators. However when calculating the thermal average we often use the coherent states to write the expression as a path integral, as in the first section with the partition function. In this case b and f become simple functions of (τ) (that is for each τ, $b(\tau)$ is just a number, not an operator). When writing the path integral we impose certain boundary conditions on these functions (as described in [1]). As a result the corresponding functions can be thought as periodic, with period β. Hence, it is possible to express them in Fourier series:

$$b(\tau) = \frac{1}{\beta}\sum_n b(i\omega_n)e^{-i\omega_n\tau}$$

where ω_n are known as Matsubara frequencies. The boundary conditions are periodic for bosons, so the bosonic Matsubara frequencies are $\omega = 2n\pi/\beta$ and antiperiodic for fermions, for which $\omega_n = (2n+1)\pi/\beta$, with $n \in \mathbb{Z}$ both cases.

Using this series in 2.18 we find the real time Green's function. Inversing we find the Matsubara frequency Green's function:

$$G(\tau) = \frac{1}{\beta}\sum_n G(i\omega_n)e^{-i\omega_n\tau} \quad , \quad G(i\omega_n) = \int_0^\beta G(\tau)e^{i\omega_n\tau}d\tau \tag{2.20}$$

In Appendix B, we define the real time/frequency analogue of this equation and we find their relationship with this imaginary time formalism. This relationship is crucial for the calculation of some quantities.

The importance of the functions defined in 2.18 lies mainly in the fact that measurable quantities can be expressed through them. An example is the local spin susceptibility which was the quantity of interest in [2].

The usual procedure to calculate Green's functions is to treat the mean-field like interaction as a perturbation to the free particle Hamiltonian. The problem is analytically solvable because in the limit $M \to +\infty$ the non-vanishing terms in the perturbation expansion can be summed. This procedure is described in detail in Appendix A, where we find the equations for Green's function, usually known as Schwinger-Dyson equations. We summarize the results of this appendix:

$$(G_B^{-1})^{ab}(i\omega_n) = (i\omega_n + \lambda)\delta^{ab} - \Sigma_B^{ab}(i\omega_n) \tag{BOS1}$$

$$\Sigma_B^{ab}(\tau) = J^2 \left[G_B^{ab}(\tau)\right]^2 G_B^{ba}(-\tau) \tag{BOS2}$$

$$G_B^{aa}(\tau = 0^-) = \kappa \tag{BOS3}$$

for bosons, and:

$$(G_F^{-1})^{ab}(i\omega_n) = (i\omega_n + \lambda)\delta^{ab} - \Sigma_F^{ab}(i\omega_n) \tag{FER1}$$

$$\Sigma_F^{ab}(\tau) = -J^2 \left[G_F^{ab}(\tau)\right]^2 G_F^{ba}(-\tau) \tag{FER2}$$

$$G_F^{aa}(\tau = 0^-) = q_0 \tag{FER3}$$

for fermions. Note that ω_n are different in each case. The equations at $\tau = 0^-$ come from the constraints we mentioned in the previous section.

2.4 Low frequency Green functions in $T = 0$

We will first focus on the spin-fluid phase. As mentioned in the end of section 2.1, in this case the dominant reason for the disorder are the quantum fluctuations and we expect the correlations to be replica diagonal.

In the limit $T \to 0^+$, both bosonic and fermionic Matsubara frequencies become continuous and

$$\frac{1}{\beta}\sum_n \to \int_{-\infty}^{+\infty} \frac{d\nu}{2\pi}$$

where we used ν for Matsubara frequencies, as we will use ω for real frequencies. Hence, the Fourier transform 2.20 becomes:

$$G(\tau) = \int_{-\infty}^{+\infty} G(i\nu)e^{-i\nu\tau}\frac{d\nu}{2\pi} \quad , \quad G(i\nu) = \int_0^{+\infty} G(\tau)e^{i\nu\tau}d\tau \tag{2.21}$$

Using these relations we write BOS2 in Matsubara frequencies:

$$\Sigma(i\nu) = J^2 \int_{-\infty}^{+\infty}\int_{-\infty}^{+\infty} G(i\nu_1)G(i\nu_2)G(i\nu_1 + i\nu_2 - i\nu)\frac{d\nu_1 d\nu_2}{4\pi^2} \tag{2.22}$$

The problem with using the functions in Matsubara frequencies is that after continuing to the entire complex plane, they have singularities on either side of the real axis. For this reason it is preferred to use the retarded Green's function defined in Appendix B. This function has singularities only bellow the real axis and it is analytic in the upper complex plane. Similarly, the advanced Green's function is analytic bellow the real axis. Functions of Matsubara frequencies (as in 2.22) come from the time-ordered Green's function, which is a combination of both the retarded (for $\tau > 0$) and the advanced (for $\tau < 0$) functions and thus non-analytic on either sides of the real axis.

In order to write 2.22 in terms of the retarded functions of real frequencies we use B.14:

$$\Sigma(i\nu) = \frac{J^2}{4\pi^2}\int_{-\infty}^{+\infty}\prod_{i=1}^{3}\left[\frac{d\omega_i}{2\pi}\rho(\omega_i)\right]\int_{-\infty}^{+\infty}\frac{d\nu_1 d\nu_2}{(i\nu_1-\omega_1)(i\nu_2-\omega_2)(i\nu_1+i\nu_2-i\nu-\omega)}$$

where $\rho(\omega) = -2\,\mathrm{Im}\,G^R(\omega)$ is the spectral function defined in B.10. The integrals in ν_1 and ν_2 can be calculated by closing the loop of integration in the upper half plane:

$$\Sigma(i\nu) = J^2\int_{-\infty}^{+\infty}\prod_{i=1}^{3}\left[\frac{d\omega_i}{2\pi}\rho(\omega_i)\right]\frac{[\Theta(\omega_3)-\Theta(\omega_1)]\,[\Theta(\omega_3-\omega_1)-\Theta(\omega_2)]}{\omega_1+\omega_2-\omega_3-i\nu}$$

The step functions appeared because the sign of the real frequencies determines whether the corresponding pole is in above the real axis (and thus contributes) or below (where there is no contribution). Since there are no integrals in Matsubara frequencies, we can

safely continue $i\nu \to \omega + i0^+$ and use Dirac's identity to get:

$$\mathrm{Im}\,\Sigma^R(\omega) = \frac{J^2}{8\pi^2}\int_{-\infty}^{+\infty} \rho(\omega_1)\rho(\omega_2)\rho(\omega_1+\omega_2-\omega)\left[\Theta(\omega_1+\omega_2-\omega)-\Theta(\omega_1)\right]\times$$

$$\left[\Theta(\omega_2-\omega)-\Theta(\omega_2)\right]d\omega_1 d\omega_2$$

The step functions determine the integration region and taking different cases about the frequencies' signs we find:

$$\mathrm{Im}\,\Sigma^R(\omega) = \frac{J^2}{8\pi^2}\int_{\Delta(\omega)} \rho(\omega_1)\rho(\omega_2)\rho(\omega_1+\omega_2-\omega)d\omega_1 d\omega_2 \tag{2.23}$$

where

$$\Delta(\omega) = \begin{cases} \omega_1,\omega_2 > 0\ ,\ \omega_1+\omega_2 < \omega & ,\text{for}\ \ \omega > 0 \\ \omega_1,\omega_2 < 0\ ,\ \omega_1+\omega_2 > \omega & ,\text{for}\ \ \omega < 0 \end{cases} \tag{2.24}$$

Moreover, we can continue BOS1 in real frequencies (replica diagonal):

$$\left[G^R(\omega)\right]^{-1} = \omega + \lambda - \Sigma^R(\omega) \tag{2.25}$$

As in [2], assuming that in low frequencies $G^R(\omega) \sim \omega^\mu$, we find from 2.23 $\mathrm{Im}\,\Sigma^R(\omega) \sim \omega^{3\mu+2}$. Using this in 2.25:

$$\omega^{-\mu} \sim \omega + \lambda - \Sigma(0) - \omega^{3\mu+2}$$

which can be true only if we neglect ω (for small frequencies), $\lambda = \Sigma^R(0)$ and $-\mu = 3\mu+2 \Rightarrow \mu = -1/2$. Hence, in small frequencies we expect $G^R(\omega) \sim \sqrt{\omega}$. Since we need the spectral function $\rho(\omega) = -2\,\mathrm{Im}\,G^R(\omega)$ to have the same sign with frequency we write:

$$G^R(\omega) = \frac{i\Lambda e^{-i\theta}}{\sqrt{\omega}} \tag{2.26}$$

where $\Lambda > 0$ and $0 < \theta < \pi/2$. We note that for $\omega < 0$ it is $\sqrt{\omega} = i\sqrt{-\omega}$ and the positivity conditions are satisfied. We will give the physical interpretation of the parameters Λ and θ in a moment. The corresponding spectral function is:

$$\rho(\omega) = 2\Lambda \begin{cases} -\cos\theta/\sqrt{\omega} & ,\omega > 0 \\ \sin\theta/\sqrt{-\omega} & ,\omega < 0 \end{cases} \tag{2.27}$$

Plugging 2.27 in 2.23 we have for $\omega > 0$:

$$\mathrm{Im}\,\Sigma^R(\omega) = \frac{J^2\Lambda^3}{\pi^2}\cos^2\theta\sin\theta\int_0^\omega\int_0^{\omega-\omega_1}\frac{d\omega_2 d\omega_1}{\sqrt{\omega_1\omega_2(\omega-\omega_1-\omega_2)}}$$

We can calculate the integrals and using

$$\int_0^{a^2} \frac{dx}{\sqrt{x(a^2-x)}} = \pi \mathrm{sgn}(a)$$

and follow the same procedure for $\omega < 0$. Finally we find:

$$\mathrm{Im}\,\Sigma^R(\omega) = \frac{J^2\Lambda^3}{\pi} \sin 2\theta \begin{cases} \cos\theta\sqrt{\omega} & ,\omega > 0 \\ -\sin\theta\sqrt{-\omega} & ,\omega < 0 \end{cases} \tag{2.28}$$

The paramater Λ can be evaluated by plugging this form and 2.26 in 2.25. For example, for $\omega > 0$:

$$\mathrm{Im}\left(\frac{\sqrt{\omega}}{i\Lambda e^{-i\theta}}\right) = -\frac{J^2\Lambda^3}{\pi}\sin 2\theta \cos\theta\sqrt{\omega} \Rightarrow \Lambda = \left(\frac{\pi}{J^2 \sin 2\theta}\right)^{1/4} \tag{2.29}$$

Therefore, the only free paramater in the low frequency bosonic Green function 2.27 is θ. We have used all Schwinger-Dyson equations so this parameter cannot be calculated. In fact, we expect to have a free parameter because of the introduction of the chemical potential λ for the constraint BOS3. This means that the parameter θ is related to the ratio κ. We recall that $\kappa = 2S/M$ with both $M, S \to \infty$, so κ can be thought as a measure for the (maximum) spin. The relation of θ and spin can be understood more clearly by calculating the local susceptibility in the low frequency limit.

2.5 Low frequency local susceptibility in $T = 0$

It is $\chi \sim \langle \mathbf{S}_i(\tau) \cdot \mathbf{S}_i(0) \rangle$ and recalling 2.16 we can write $\chi(\tau) = Q^{aa}(\tau) = G(\tau)G(-\tau)$. These imaginary time Green's functions can be calculated by transforming 2.27 using B.12. For $T \to 0^+$ it is $\left[e^{-\beta\omega} - 1\right]^{-1} \to \Theta(\omega)$, so:

$$G(\tau) = \int_0^{+\infty} \rho(\omega) e^{-\omega\tau} \frac{d\omega}{2\pi} = -\frac{\Lambda}{\sqrt{\pi\tau}} \cos\theta \tag{2.30}$$

The same can be done for negative imaginary time argument:

$$G(-\tau) = -\int_{-\infty}^{0} \rho(\omega) e^{\omega\tau} \frac{d\omega}{2\pi} = -\frac{\Lambda}{\sqrt{\pi\tau}} \sin\theta \tag{2.31}$$

From which we can find the local susceptibility:

$$\chi(\tau) = \frac{\Lambda^2 \sin 2\theta}{2\pi|\tau|} = \frac{1}{2J|\tau|}\sqrt{\frac{\sin 2\theta}{\pi}} \tag{2.32}$$

Susceptibility is the first measurable quantity that we calculated here. If our model corresponded to a real system, we could apply an external magnetic field and measure it. The magnetic field causes a magnetization to the material and susceptibility measures the response: $\chi = \partial M/\partial B$. In normal paramagnetic materials we usually assume $M \propto B$ and χ reduces to the proportionality constant.

Clearly M is dependent on the ability of spins to align and we expect it to be larger when we have order. High temperatures generally destroy order through thermal fluctuations, so χ reduces in respect to T. Curie-Weiss is a common law for this, according to which[2] $\chi \sim T^{-1}$. This sometimes is generalized to $\chi \sim T^{-\gamma}$ where $\gamma > 0$ is the critical exponent. According to 2.32 the corresponding law for our model is $\chi \sim \int_0^\beta \chi(\tau)d\tau \sim \ln T$ which diverges slower than $T^{-\gamma}$ for any $\gamma > 0$ [4]. This is characteristic of the spin liquid disorder which is maintained even at $T \to 0^+$ as it caused by quantum, not thermal, fluctuations.

We also expect the susceptibility to increase in respect to the total spin S. From 2.32 we can see that χ is an increasing function of θ for $0 < \theta < \pi/4$. This means that we expect θ to be an increasing function of spin in this region. However, this changes for $\pi/4 < \theta < \pi/2$ where the susceptibility becomes a decreasing function of θ. According to [2] this signals a phase transition from the phase transition, meaning that only $0 < \theta < \pi/4$ corresponds to the spin liquid phase for the bosonic model.

This was further explained in more recent publications, specifically in [4], where an equation between κ and θ was derived:

$$\kappa = \frac{1}{4} - \frac{\theta}{\pi} + \frac{\cos 2\theta}{4} \tag{2.33}$$

Such equations are usually called Luttinger relations and they are derived by imposing the constraints like BOS3. We did not include the derivation in this section because it is given in detail in an appendix of [4] and we usually include the calculations that are ommited in the papers. If we plot the RHS of 2.33 for $0 \leq \theta \leq \frac{\pi}{2}$ we find that it is positive

[2] There are ferromagnetic materials for which there is a critical temperature T_c below which they maintain their magnetic order. We do not expect such behavior at least in the strongly disordered spin liquid phase and we assumed $T_c = 0$.

for $\theta < \frac{\pi}{4}$ and negative $\theta > \frac{\pi}{4}$. This is another way of identifying the phase change, as the equation is not solvable for $\theta > \frac{\pi}{4}$ because $\kappa = 2S/M$ is always positive.

2.6 Fermionic case

The work of the two previous sections can be repeated for the fermionic representation. In fact, because of the similarity of the Schwinger-Dyson equations BOS1-BOS3 with FER1-FER3 we expect almost the same results. However there is a major difference, as the fermionic case does not exhibit the spin-glass phase - the quantum fluctuations are very strong and we stay at the disordered spin fluid phase for all values of q_0.

Mathmatically the difference comes from the spectral function positivity conditions, as in the fermionic case we have $\rho(\omega) > 0$ for all $\omega \in \mathbb{R}$. We write:

$$G^R(\omega) = \frac{A}{\sqrt{\omega}} e^{-i(\pi/4+\theta)} \tag{2.34}$$

from which:

$$\rho(\omega) = \frac{2A}{\sqrt{|\omega|}} \begin{cases} \sin\left(\frac{\pi}{4}+\theta\right) & ,\omega > 0 \\ \cos\left(\frac{\pi}{4}+\theta\right) & ,\omega < 0 \end{cases} \tag{2.35}$$

which satisfies the positivity conditions for $A > 0$ and $|\theta| \leq \pi/4$. The self energy can be found using an equation like 2.23, noting the minus sign that exists in FER2. Apart from that and the differences in the trigonometric factors, the calculation is identical to the bosons and we find:

$$\operatorname{Im}\Sigma^R(\omega) = -\frac{J^2A^3}{\pi}\sqrt{|\omega|}\cos 2\theta \begin{cases} \sin\left(\frac{\pi}{4}+\theta\right) & ,\omega > 0 \\ \cos\left(\frac{\pi}{4}+\theta\right) & ,\omega < 0 \end{cases} \tag{2.36}$$

and from FER1:

$$A = \left(\frac{\pi}{J^2\cos 2\theta}\right)^{1/4} \tag{2.37}$$

The Green's function (as in 2.30) is:

$$G(\tau) = \frac{A}{\sqrt{\pi J|\tau|}} \begin{cases} -\sin\left(\frac{\pi}{4}+\theta\right) & ,\tau > 0 \\ \cos\left(\frac{\pi}{4}+\theta\right) & ,\tau < 0 \end{cases} \tag{2.38}$$

Finally the susceptibility is:

$$\chi(\tau) = \frac{1}{2J|\tau|}\sqrt{\frac{\cos 2\theta}{\pi}} \tag{2.39}$$

We recall that the limits now are $|\theta| \leq \pi/4$ and we observe that the susceptibility is an increasing function of θ on this whole range. This is in contrast with the bosonic case where we had a change at the susceptibility behavior as a function of θ. The monotonic χ corroborates the fact that we have only spin fluid phase in the fermionic representation.

Moreover, the Luttinger relation for this case is (again from [4]):

$$q_0 = \frac{1}{2} - \frac{\theta}{\pi} - \frac{\cos 2\theta}{4} \tag{2.40}$$

For $|\theta| \leq \pi/4$ the right hand side is an one to one function to $0 \leq q_0 \leq 1$, which is exactly the allowed region for q_0. This indicates that we always have a unique solution which apparently is on the spin fluid phase.

2.7 Numerical solutions

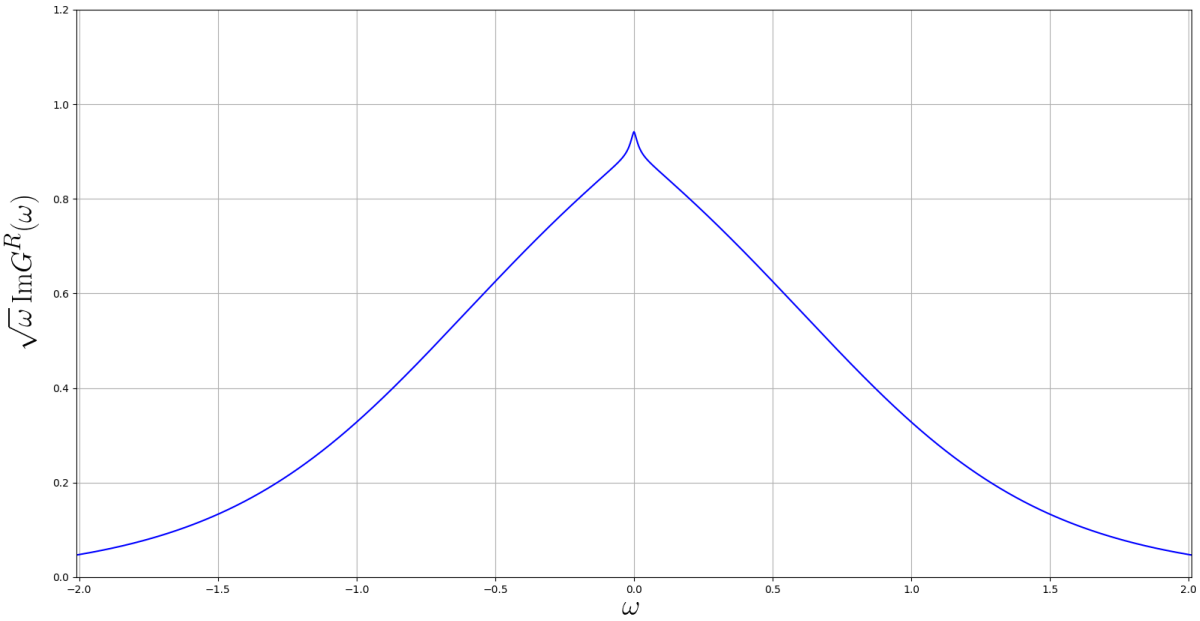

FIGURE 2.1: Spectral function obtained numerically for fermionic case. This diagram is qualitatively in agreement with the one included in [2].

In [2] the low frequency solutions which we found in the previous sections were extended numerically in higher frequencies. In Appendix C we analyze a way to do this and give the corresponding code. We applied this code for the fermionic case and we plotted the spectral function in Figure 2.1 rescaled to match the low frequency value of $(\pi/2)^{1/4}$ at

$\omega = 0$. The same figure is included in [2]. We note that this is the case where the spectral function is even, which means that $\theta = 0$ (for fermions).

2.8 Comment on positivity conditions

Comparing the results of the bosonic and fermionic case we concluded that the main difference is the existence of a spin glass phase in the former. We argued that this is apparent from the θ dependence of the local susceptibility. Of course this is not a proof of existence of the spin glass phase, but it indicates a change of behaviour of the bosonic model in large spin κ.

Mathematically this result comes from the difference in the trigonometric functions which appear in equations 2.32 and 2.39. We recall that these functions are a result of the different spectral function's positivity conditions, namely because we demanded $\rho(\omega) > 0$ for fermions whereas $\omega\rho(\omega) > 0$ for bosons. Therefore, the reason for the different behavior of the two models must be hidden in these conditions.

These conditions are a straightforward result of the Lehmann representation B.11 for both the bosonic ($p = 1$) and the fermionic ($p = -1$) case. It is also instructive to write the average particle number for a general system as an integral of the spectral function. This equation can be found using the Lehmann representation:

$$\langle N \rangle = \int_{-\infty}^{+\infty} \frac{\rho(\omega)}{e^{\beta\omega} - p} \frac{d\omega}{2\pi} \to -\frac{1}{p} \int_{-\infty}^{0} \rho(\omega) \frac{d\omega}{2\pi}$$

where we took the limit $T \to 0^+$ and $p = \pm 1$ for bosons/fermions. The weight of ρ in the first integral is the known Bose-Einstein/Fermi-Dirac distributions. From this relation we observe that the physical condition $\langle N \rangle > 0$ leads to $\rho(\omega) < 0$ for bosons and $\rho(\omega) > 0$ for fermions for $\omega < 0$.

We presented this argument in order to suggest that the positivity conditions somehow contain the informations from the corresponding bosonic and fermionic distributions. The physics of these distributions at $T = 0$ is that they allow condensation in the state with the lowest energy for bosons but not for fermions. In a way, the fermionic system behaves more quantum mechanically, as the Pauli principle, which is clearly a quantum mechanical property, restricts the distribution.

We recall that this property is the reason why in the particle in a box fermionic model we have non zero pressure even at $T = 0$. Despite there are no thermal fluctuations at zero temperature, the quantum fluctuations in fermions are strong enough to lead to finite pressure. In a similar essence, in our model these quantum fluctuations lead to the disordered spin fluid phase and suppress the spin glass phase for any value of q_0.

The analogy we are trying to establish here might not be so clear for the SY model, as fermions and bosons are inserted artificially (mathematically) as representation of spins and they do not constitute the actual system. The difference in physics is observed because the fermionic representation is used in the limits $M \to +\infty$ and S constant, while the bosonic representation is for the limits $M, S \to +\infty$ with $2S/M = \kappa = \text{const}$. In this sense, bosonic limits are more classical than fermionic because of the $S \to +\infty$ which approaches classical physics as it makes the commutator of spin to approach zero.

2.9 Finite temperature

There is an interesting symmetry of the Schwinger-Dyson equations in the low frequency limit, which allows us to extent the zero temperature solutions to finite temperature. First of all, since we interchanged the initial condition $G(\tau = 0^-) = q_0$ with the Luttinger relation 2.40 we may neglect the chemical potential. Moreover, in the low frequency limit we may neglect the $i\omega_n$ term. The equations then are:

$$\left\{ \begin{array}{c} G(i\omega)\Sigma(i\omega) = -1 \\ \Sigma(\tau) = -J^2 G^2(\tau) G(-\tau) \end{array} \right\}$$

and using the Fourier transforms 2.20 we can write one equation that contains only the Green function:

$$\int_0^{+\infty} G(\tau_2 - \tau_1) G^2(\tau_3 - \tau_2) G(\tau_2 - \tau_3) d\tau_2 = \frac{1}{J^2} \delta(\tau_1 - \tau_3) \tag{2.41}$$

This equation is symmetric under the transformation:

$$\tau \to f(\tau) \quad , \quad G(\tau_2 - \tau_1) \to [f'(\tau_1) f'(\tau_2)]^{-1/4} \, G\left(f(\tau_2) - f(\tau_1)\right) \tag{2.42}$$

That is, its form does not change when doing the transformation. We can prove this by changing the variable $\tau_2 \to f(\tau_2)$ in the integral and using a property of delta function in

the right hand side:

$$\delta\left(f(\tau_1)-f(\tau_3)\right)=\frac{\delta(\tau_1-\tau_3)}{f'(\tau_1)}$$

Here we treated τ_1 as a variable and τ_3 as a constant. Of course if we interchange them the result is the same as the existence of delta means that they are equal. Also, we asumed that f is a bijective function and thus the delta argument is zero only if $\tau_1=\tau_3$.

In case of finite temperature, equation 2.41 is still valid if we replace infinity with β. We can then do a transformation like the above with a proper choice of f, in order to recover the infinity without changing the equations form. The appropriate f must map $(0,+\infty)$ to $(0,\beta)$ and can be for example $f(\tau)=\tan(\pi\tau/\beta)$. Therefore the Green function in non zero temperature is:

$$G_\beta(\tau)=\left[f'(\tau)f'(0)\right]^{1/4}G\left(f(\tau)\right)=G\left(\tan\frac{\pi\tau}{\beta}\right)\sqrt{\frac{\pi}{\beta\cos(\pi\tau/\beta)}}$$

where G is the $T=0$ function which is given by 2.38. Hence:

$$G_\beta(\tau)=\frac{A}{\sqrt{\beta J|\sin(\pi\tau/\beta)|}}\begin{cases}-\sin\left(\frac{\pi}{4}+\theta\right) & ,0<\tau<\beta\\ \cos\left(\frac{\pi}{4}+\theta\right) & ,-\beta<\tau<0\end{cases}\tag{2.43}$$

The problem with 2.43 is that it does not satisfy the antiperiodic fermionic boundary conditions $G_\beta(\tau+\beta)=-G_\beta(\tau)$ because of change in the branch. This is caused by θ, as the problem is absent when $\theta=0$ ($q_0=1/2$), therefore it must be related with the introduction of the chemical potential and the spectral asymmetry that this causes [4][10].

This problem can be fixed by using the gauge symmetry [6] that exists in the complex model (like SY - but does not exist on Majorana fermion SYK). This symmetry allows us to write another factor g in the transformation 2.42:

$$G(\tau_2-\tau_1)\to\left[f'(\tau_1)f'(\tau_2)\right]^{-1/4}\frac{g(f(\tau_1))}{g(f(\tau_2))}G\left(f(\tau_2)-f(\tau_1)\right)\tag{2.44}$$

This allows us to rewrite 2.43 as:

$$G_\beta(\tau)=\frac{Ag(\tau)}{\sqrt{\beta J|\sin(\pi\tau/\beta)|}}\begin{cases}-\sin\left(\frac{\pi}{4}+\theta\right) & ,0<\tau<\beta\\ \cos\left(\frac{\pi}{4}+\theta\right) & ,-\beta<\tau<0\end{cases}\tag{2.45}$$

Requiring $F(\tau+\beta)=-F(\tau)$ for $-\beta<\tau<0$ we find:

$$\cos\left(\frac{\pi}{4}+\theta\right)g(\tau)=\sin\left(\frac{\pi}{4}+\theta\right)g(\tau+\beta)\Rightarrow\frac{g(\tau)}{g(\tau+\beta)}=\tan\left(\frac{\pi}{4}+\theta\right)\ \forall\ -\beta<\tau<0$$

In order for this to be valid for all τ we need to cancel it from the left hand side and for this reason we use an exponential form $g(\tau) = e^{-a\tau}$. Plugging this into the equation we find:

$$a = \ln\left[\tan\left(\frac{\pi}{4} + \theta\right)\right] \tag{2.46}$$

and the correct form of the Green's function is:

$$G_\beta(\tau) = \frac{Ae^{-a\tau}}{\sqrt{\beta J|\sin(\pi\tau/\beta)|}} \begin{cases} -\sin\left(\frac{\pi}{4}+\theta\right) & ,0 < \tau < \beta \\ \cos\left(\frac{\pi}{4}+\theta\right) & ,-\beta < \tau < 0 \end{cases} \tag{2.47}$$

2.9.1 More on gauge symmetry

The fact that we are able to use the additional g function in transformation 2.44 can be justified as follows: We can think of the Hamiltonian 2.3 in real time, that is the Grassmann variables after doing the coherent state path integral are complex functions $c_{i\alpha} = c_{i\alpha}(t)$. We can then do a gauge transformation analogous to field theory:

$$c_{i\alpha}(t) \to c'_{i\alpha}(t) = e^{-i\theta_i(t)} c_{i\alpha}(t) \tag{2.48}$$

Clearly 2.3 is invariant under this transformation as for every site i it also contains its complex conjugate and phase terms cancel. This symmetry always exists in the problem, independently of temperature or low/high frequency, in contrast to the conformal symmetry which breaks in high frequencies where the term $i\omega_n$ is not negligible. However this symmetry does not hold in real models like the Majorana fermion SYK. It also does not generally hold [6] in the complex SY 4.3 with which we will work in Chapter 4, because there the Hermitian conjugate in the Hamiltonian is on different sites.

Taking into account the definition B.3 of the retarded Green's function in real time, we can see that under 2.48 it transforms as $G^R \to G^{R'}$ with:

$$G^{R'}(t_2 - t_1) = \frac{1}{M}\sum_{\alpha=1}^{M} \left\langle \left\{ c^\dagger_{i\alpha}(t_1) e^{i\theta_i(t_1)}, e^{-i\theta_i(t_2)} c_{i\alpha}(t_2) \right\} \right\rangle = \frac{e^{-i\theta_i(t_2)}}{e^{-i\theta_i(t_1)}} G^R(t_2 - t_1) \tag{2.49}$$

The multiplicative factor is the analogue of $g(\tau_2)/g(\tau_1)$ in 2.44. The difference is that in real time g will be real functions in contrast with the common imaginary phase gauge term of 2.49.

Chapter 3

Chaos and Out-of-time-ordered Correlators

3.1 Chaos in classical systems

The main problem in the theory of dynamical systems is equations of the form $\dot{\mathbf{x}}(t) = \mathbf{F}(\mathbf{x}, t)$ where $\mathbf{x} \in \mathbb{R}^d$. Usually the goal is to describe the time evolution of a quantity that follows an ordinary differential equation law and it is easy to transform an equation of any order into this vector form.

In most cases such equations cannot be solved analytically. Hence, the theory focuses on describing the systems near equilibrium points, that is points where $\mathbf{F} = 0$ or equivalently if $\mathbf{x}$ is found at such a point then it will stay there forever. Fortunately, nature seems to like equilibrium as systems tend to move to equilibrium points after some time, so it is enough to know the system's behavior only near these points (called attractors in the phase space).

When $d = 1, 2$ the behavior of systems is relatively simple to understand as the only[1] possible attractors are fixed points, that is points which the system tend to approach as $t \to +\infty$, or limit cycles which correspond to periodic orbits. However, the situations is more complicated when $d \geq 3$, when the so called strange attractors appear. We can naively describe a strange attractor like a limit cycle (a point that the system evolves

[1] Excluding cases where the system goes to infinity, like $\dot{x} = x$.

around it) but with a fractal structure. Unlike, limit cycles the trajectory is not periodic or equivalently we can not cross the same point twice in the phase space[2].

Suppose now that we start from two nearby points $\mathbf{x}_0$ and $\mathbf{x}_0 + \mathbf{d}_0$ with $|\mathbf{d}_0| \ll 1$ and we observe the corresponding evolutions. Dynamical systems are deterministic so, at least numerically, we are able to predict the evolution. Clearly, in the case of fixed points and limit cycles we expect the distance $|\mathbf{d}(t)|$ between the two orbits to approach zero or a constant value. However the behavior in strange attractors is not straightforward.

Analyzing numerically the most famous system with a strange attractor, Lorenz's equations, one finds that $|\mathbf{d}(t)| \sim |\mathbf{d}_0| e^{\lambda t}$ [21]. According to this result, no matter how close two trajectories start, if $\lambda > 0$ we expect them to separate at some future time. Equivalently, the system is highly sensitive on initial conditions, as a small change may cause a completely different outcomes, something known as butterfly effect.

The importance of this effect in physical systems comes from its combination with uncertainty in initial conditions. This uncertainty exists in every system and even if we narrow it to the quantum (Heisenberg) limit, the exponential nature of the increase in distance between the trajectories will make it significant after some appropriate time. The exact amount of this time depends of course on the starting uncertainty, our error tolerance and λ, which somewhat quantifies how fast the system separates neighboring trajectories. This parameter is called Lyapunov exponent and we can define it as:

$$\lambda = \lim_{t \to +\infty} \lim_{|\mathbf{d}_0| \to 0} \left[\frac{1}{t} \ln \left(\frac{|\mathbf{d}(t)|}{|\mathbf{d}_0|} \right) \right] \tag{3.1}$$

Chaos in classical systems is usually defined using this Lyapunov exponent. A chaotic system must be deterministic but sensitive on initial conditions, meaning that nearby trajectories separate exponentially fast in time ($\lambda > 0$).

3.2 Out-of-time-ordered correlator

Generalizing chaos concepts in quantum mechanics is far from trivial. In quantum mechanics we describe systems by an abstract vector $|\psi\rangle$, in contrast with the classical (x, p) phase space description. The major difference is that the evolution of $|\psi\rangle$ is governed

[2]Having in mind that we cannot cross the same point twice and that curves in phase space are continuous, it is easy to understand, because of topological reasons, why we cannot have a strange attractor in 1 or 2 dimensions. This is known as the Poincare-Bedixson theorem.

by Schrodinger's equation, which being first order in time, is fairly simple in comparison with classical evolution laws and it cannot exhibit chaos. The question then is, since all systems are fundamentally quantum mechanical, why chaos exists? It is not the purpose of this work to answer such questions, although a simple reason could be that $|\psi\rangle$ might not be chaotic, but it is not a measurable quantity either.

The concept of quantum chaos in general has been a topic of interest for several years. Most of relevant work is on the semi-classical limit and on quantum systems which have a chaotic classical counterpart. A famous example is the quantum kicked rotor, a particle on a ring which moves under the influence of a field that is enabled periodically in time. Here we are interested in a recent development in the field of quantum chaos, according to which the Lyapunov exponent for a quantum system can be calculated from the growth rate of a specific correlator.

According to [15] such quantity can be related to the commutator of two arbitrary observables (Hermitian operators):

$$C(t) = -\left\langle [W(t), V(0)]^2 \right\rangle \tag{3.2}$$

The use of the commutator can be intuitively reasoned if W and V represent classical quantities, like position or momentum. In fact this was the case in [22] which was also the first appearance of a quantity like C. The authors were interested in the validity of the quasiclassical method in calculating quantum expectation values in a system of almost free electrons interacting with impurities. They calculated quantum mechanically the values of $\langle p^2(t)p^2(0)\rangle$ and $\langle p(t)p(0)p(t)p(0)\rangle$ and they observed that although the first result could be obtained using classical methods, this was not the case for the second. This indicated the importance of the order of operators in the expectation value. Clearly the difference between this two quantities is related to C of 3.2, as if we expand the square and use a trace identity we have:

$$C(t) = 2\left\langle W^2(t)V^2(0)\right\rangle - 2\left\langle W(t)V(0)W(t)V(0)\right\rangle \tag{3.3}$$

Therefore this difference for the case of electrons was related to the fact that momentum operators do not commute at different times, because of the interaction with impurities. In [22] they continued by estimating the expectation value of the commutator in the semi-classical limit. This is probably the best way to establish the analogy between C and classical chaos. In this limit we can interchange the commutator with a Poisson

bracket:

$$-i[W,V] \to \{W,V\} = \frac{\partial W}{\partial x(0)}\frac{\partial V}{\partial p(0)} - \frac{\partial W}{\partial p(0)}\frac{\partial V}{\partial x(0)}$$

and applying this for $W(t) = x(t)$, $V(0) = p(0)$ we have:

$$-\left\langle [x(t), p(0)]^2 \right\rangle \approx \left\langle \left(\frac{\partial x(t)}{\partial x(0)}\right)^2 \right\rangle \sim e^{2\lambda t}$$

since this partial derivative measures changes of the final position $x(t)$ in respect to changes of initial condition $x(0)$, as in 3.1. Hence, we might expect $C(t)$ to increase exponentially at long times.

According to the results of [22], $\langle p^2(t)p^2(0)\rangle$ converges to a constant value at long times, while $\langle p(t)p(0)p(t)p(0)\rangle$ vanishes exponentially as $t \to +\infty$. This means that the increase observed in $C(t)$ is caused by the decrease of the out-of-time-ordered correlator (OTOC), that is the second term in 3.3. This observation gives the quantum butterfly effect definition given in [15], according to which $C(t)$ should become of order $2\langle W^2\rangle\langle V^2\rangle$ at large times.

In some context the vanishing out-of-time-ordered correlator is directly related to sensitivity in initial conditions. Suppose we start from $|\psi\rangle$, act with V, evolve for time t, then act with W and return to $t = 0$. Mathematically:

$$|\psi\rangle \to |\psi_1\rangle = U(0,t)WU(t,0)V|\psi\rangle = W(t)V(0)|\psi\rangle$$

Suppose now that we reverse this procedure so that we first make the evolutions and act with W and then with V:

$$|\psi\rangle \to |\psi_2\rangle = VU(0,t)WU(t,0)|\psi\rangle = V(0)W(t)|\psi\rangle$$

Then the OTOC (second term in 3.3) is the same with the product $\langle\psi_2|\psi_1\rangle$. This product somewhat quantifies how similar the two states are[3]. If this vanishes it means that if we do the perturbation V before evolving acting with W, then we get a completely different state, characteristic of the butterfly effect.

[3] A known measure of how related two quantum states are is fidelity: $|\langle\psi_2|\psi_1\rangle|^2$.

3.3 Scrambling of information

The main purpose of presenting the fact of the previous section is not to rigorously prove that $C(t)$ is a fine measure of chaos, but rather to intuitively connect this quantity with some basic classical chaos concepts. Up to now, there is no clear evidence that the commutator or the OTOC is in agreement with previous developments in the field of quantum chaos. On the contrary, it seems that the Lyapunov exponent that can be calculated from these correlators is different from the classical exponent in systems like the kicked rotor [17]. This is corroborated in [23] where it is stated that the quantity that we calculate is not exactly the classical Lyapunov exponent.

Based on these, we believe that the main purpose of the work on out-of-time-ordered correlators is not to find a correct description of quantum chaos, but rather to find the connections with scrambling of information either from quantum information or black-hole physics perspective. In simple words, we are interested in how fast information encoded in a specific part of a system spreads to the rest of it. A very instructive model for the study of such effects is an ensemble of qubits interacting with an Ising Hamiltonian, proposed in [24]. In order to present this system we need to recall some elementary concepts:

A composite quantum system is constituted by several subsystems so that the total Hilbert space can be written as $\mathcal{H} = \mathcal{H}_A \otimes \mathcal{H}_B \otimes ....$ If the total system is in a state $|\Psi\rangle$, then the density matrices for the subsystems are given by tracing out the rest degrees of freedom: $\rho_A = \mathrm{Tr}_{BCD...} |\Psi\rangle \langle\Psi|$. If $|\Psi\rangle$ is an entangled state, then $\rho_A, ...$ are not pure states and cannot be written as kets.

Non-pure states are usually thought as ensembles: apart from the usual quantum randomness there is randomness that comes from classical statistics. By quantum randomness we mean that while being in a state $|\psi\rangle$ we do not know the value of a specific observable. By statistical randomness we mean that we do not even know if we are in state $|\psi\rangle$ or in another state: $\rho = \sum_k p_k |k\rangle \langle k|$.

A famous state is the canonical ensemble: $\rho = e^{-\beta H}$. In general this cannot be written as a pure state (ket): $\rho \neq |\psi\rangle \langle\psi|$. However we can purify this state if we consider it as a subsystem of a larger (doubled) system. This construction is known as the thermofield double:

$$|\Psi\rangle = \frac{1}{\sqrt{Z}} \sum_n e^{-\beta E_n/2} |n_L\rangle |n_R\rangle \tag{3.4}$$

where L, R stand for left and right system. If we trace out right, then left is in the canonical ensemble state. The use of the square root of the probability $e^{-\beta E_n}/Z$ in 3.4 is familiar from Schmidt's decomposition. Apart from this technical points, the thermofield double seems to be crucial in the interplay between information theory/black hole physics. [15][23][24]

A quantity that usually measures correlations between subsystems from the information perspective is mutual information. If A, B are subsystems of a larger this quantity is defined as $I = S_A + S_B - S_{A\cup B}$, where S_X is the Von Neumann entropy of subsystem X. This is the quantum mechanical analogue of Shannon entropy and I is the quantum analogue of classical mutual information which aims to answer the question: If we have access only to A, how much can we learn for B.

The Von Neumann entropy can be calculated as $S_X = \mathrm{Tr}\,(\rho_X \ln \rho_X)$. This entropy is also an entanglement meausure for $|\Psi\rangle$. For example if the system in $|\Psi\rangle$ is constituted by two subsystems A and B, then it is entangled if and only if $S_A > 0$ and the higher S_A is, the more entangled the state is[4].

In the qubit example of [24], they prepare a thermofield double state for an Ising Hamiltonian with 10 qubits[5] in the left and 10 in the right part. The Hamiltonian has a specific form for the system to be non-integrable, which we do not include here as we are mainly interested in qualitative results. The fifth qubit of the left counterpart is perturbed by σ_z in time t_w in the past so that the $t = 0$ state becomes[6]: $|\Psi'\rangle = e^{-iH_L t_w}\sigma_z^{(5,L)} e^{iH_L t_w}|\Psi\rangle$. Clearly this perturbation alters the state because $\sigma_z^{(5,L)}$ does not commute with the Hamiltonian.

In order to study how the state is altered they calculate a mutual information. Part A is the first two qubits of left and part B is the same qubits of right. Note that the perturbation was on the fifth qubit which is not included in these parts. The mutual information of A and B is ploted as a function of t_w (Figure 3.1 blue line). The red line is a spin-spin correlation function that shows a similar behavior.

We find that mutual information remains constant for some time after which it drops to zero. The constant part corresponds to the mutual information of the thermofield double state 3.4 which is constant and exists because the perturbation done in the fifth qubit

[4]For example, singlet states which are known to be maximally entangled have $S_A = \ln 2$, the maximum possible entropy for bipartite systems.

[5]Qubits can be thought as particles with spin-1/2, frozen in sites and interacting only because of their spin.

[6]The left operators act as $V^L \otimes 1^R$ in the total Hilbert space.

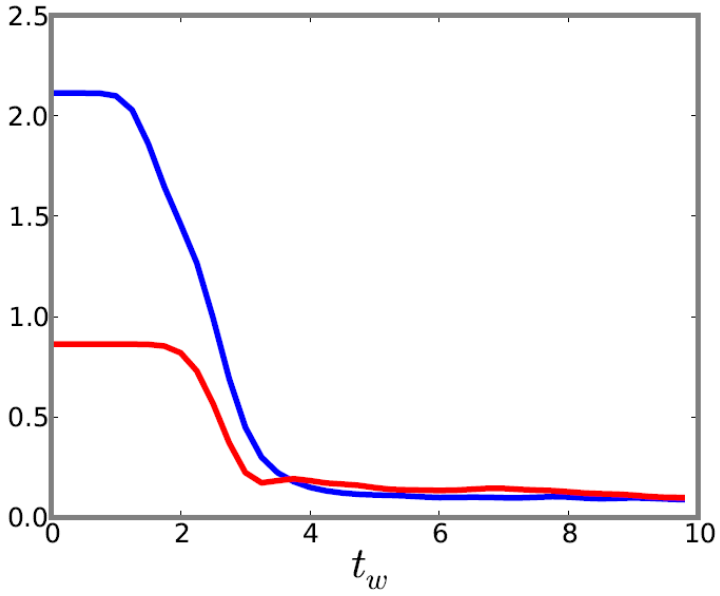

FIGURE 3.1: Mutual information between the first two qubits of left and right (blue) and correlation between the first right and first left qubit (red). This figure was copied by [24] where it was calculated numerically.

needs some time to propagate (due to the action of the evolution operators e^{-itH}) to the first two qubits. However, after this time passes, there is some significant change in the system that causes mutual information to approach zero.

Recall the physical interpretation of mutual information: If we access the first two qubits in R, can we learn anything about the same qubits in L? For the thermofield double state it is $I > 0$ and apparently we can learn something. On the other hand, for the slightly perturbed (even far from the qubits we are interested in) state $I \to 0$ and this ability is lost - the local correlations are destroyed or equivalently information is scrambled.

This behavior seems to have some similarities with the butterfly effect defined in the previous sections: the small perturbation changed drastically the correlations between different parts of the system. Also, the vanishing mutual informations forms some resemblance to the vanishing OTOC. The butterfly effect is of course a property of the Hamiltonian. A different (probably integrable) Hamiltonian here would not cause scrambling. In [23] this equivalence is studied in more detail for the case of unitary quantum channels and they prove rigorously that butterfly effect (chaotic Hamiltonian) implies scrambling. The va

Figure 3.1 also introduces the concept of scrambling time. The effect does not happen instantly, but after some time related to how fast the perturbation propagates to the subsystems we measure. We expect this time to depend on the size of the system a

propagation will be slower for larger systems (with more qubits). According to [15] the scrambling time is $t_* \sim \ln N$ where N is the number of qubits. The use of logarithm here is another similarity to classical chaos in 3.1.

3.4 A bound on chaos

Loss of information in black holes is a subject of interest for many years, leading to the famous black hole information paradox. This puzzle arises when one is interested in a quantum description of black holes, as the unitarity of quantum theories does not allow loss of information. However, it allows scrambling of information and it seems that black holes are pretty good at this. Instead of destroying information, black holes scramble it in a way that makes it practically unaccessible (or is it accessible? [25]).

As in information theory, scrambling in black holes was connected to butterfly effect and sensitivity to perturbations. A pedagogical explanation is given in [18]. A characteristic surface of a black hole is the horizon. This is the point of no return: if someone crosses the horizon he may not feel anything instantly, but eventually gravitational effects will cause his collapse to the singularity. Assume an unperturbed black hole and a photon W that at $t = 0$ passes just outside the horizon, but it is not captured. Now imagine that the same was perturbed by absorbing a photon at $t = -t_w < 0$ and this caused a slight expansion of the horizon. Now at $t = 0$ W will pass and the black hole will capture it.

A lot of work, including [24], focused on quantifying this scrambling in black holes using quantities like mutual information. Using holographic techniques, the mutual information was found $I \sim e^{2\pi t_w/\beta}/S$. Here β is the inverse temperature of the black hole. S. Hawking introduce the concept of temperature for black holes in order to find their quantum mechanical description. As every object with temperature, black holes radiate the famous Hawking radiation as they evaporate. The information that was absorbed by the black hole is included in this radiation but it is scrambled and cannot be easily read.

The introduction of temperature gives the black hole a many-body system character and an entropy can be calculated for the system. However, there is a difference as classical many-body systems have an extensive entropy $S \sim N$, while for black holes $S \sim N^2$ (for a very interesting and easy to understand clarification of this see [26] about D-branes). In any case S increases with the size of the system and this with the exponential decay of the mutual information gives the logarithmic law for the scrambling time: We need

$e^{2\pi t_w/\beta}/S$ to become of order one and this happens for time

$$t_* \sim \frac{\beta}{2\pi} \ln S \tag{3.5}$$

which also is of order $\ln N$ as in the qubit model. This is usually called the fast scrambling time.

Recalling the qualitative equivalence between mutual information and the OTOC as a diagnostic of the butterfly effect, the exponential defines the analogue of Lyapunov exponent. Here $\lambda_{\mathrm{L}} = 2\pi/\beta$. Therofore, equation 3.5 can be written as $t_* \sim \ln S/\lambda_{\mathrm{L}}$. This has a simple interpretation: a large system has higher S and scrambles slower (recall how propagation effects delay scrambling). Also, the higher the Lyapunov exponent, the more chaotic the system which makes scrambling faster.

The size of the system is pretty straightforward, but what do we know about the chaos measure λ_{L} and what is so special about the black hole value $\lambda_{\mathrm{L}} = 2\pi/\beta$? This was answered by [15] where the quantum bound of the Lyapunov exponent was established. The proof is basically based on mathematical arguments, specifically that the OTOC function $F(t) = \langle W(t)V(0)W(t)V(0)\rangle$ is analytic on a strip of width β in the complex time plane and that its complex absolute value is bounded by one. The result is a universal bound for the Lyapunov exponent by its black hole value:

$$\lambda_{\mathrm{L}} \leq \frac{2\pi}{\beta} = \frac{2\pi k_B T}{\hbar} \tag{3.6}$$

where we restored the constants for completeness. This result combined with 3.5 means that black holes are indeed the fastest scramblers. If we needed a quantum memory to storage information and maintain it for long time, then a black hole would be the worst choice, as it would scramble it as fast as possible!

According to the arguments presented above, black holes scramble with a very specific rate. Therefore, if we need a large N system dual to a black hole, it must certainly saturate 3.6. It has also been speculated that saturation of this bound sufficient for a large N system to have a gravity dual. [15] The Majorana SYK model proposed by A. Kitaev and the complex SYK model which is the subject of the next chapter are two simple examples of large N models that saturate the Lyapunov exponent bound.

Chapter 4

Chaos in Complex SYK

In Chapter 3 we described how the exponent in the N^{-1} term of the OTO correlator expansion is an indication of chaos. Originally this behavior was observed to exist in the model proposed by Kitaev [7][8][9]):

$$H = \frac{1}{N^{3/2}} \sum_{jklm} J_{jklm} \psi_j \psi_k \psi_l \psi_m \tag{4.1}$$

where ψ_i are Majorana fermion operators and J_{ijkl} are random variables with zero mean and variance J^2 (some normalization constants are omitted). This model can generally be thought as a simplification of the fermion representation of the SY model which we analyzed in Chapter 2 and is described by the Hamiltonian 2.3:

$$H = \frac{1}{\sqrt{NM}} \sum_{i,j=1}^{N} \sum_{\alpha,\beta=1}^{M} J_{ij} c_{i\alpha}^{\dagger} c_{j\beta}^{\dagger} c_{i\beta} c_{j\alpha} \tag{4.2}$$

The simplification comes mainly from the fact that only one limit $N \to +\infty$ shall be taken to access the required state, while in the SY model we had to take $N \to +\infty$ first and then $M \to +\infty$. These limits are required because we need to suppress the spin-glass phase and access a state with strong quantum fluctuations. We recall that this happens in the fermion representation of the SY model.

Another simplification is the use of the Hermitian Majorana operators instead of complex fermions. However, the chaos exponent seems to be independent of this, as it still exists

at the complex generalization of the SYK model, proposed by Sachdev in [6]:

$$H = \frac{1}{(2N)^{3/2}} \sum_{i,j,k,l=1}^{N} J_{ijkl} c_i^\dagger c_j^\dagger c_k c_l \tag{4.3}$$

In this model J_{ijkl} is still random, as in the real SYK, but they can be complex numbers with antisymmetric properties: $J_{ijkl} = -J_{jikl} = -J_{ijlk}$, $J_{ijkl} = J^*_{klij}$ and $\overline{|J_{ijkl}|^2} = J^2$.

In this chapter we will present the calculation of the OTO correlator for 4.3. Of course such calculation has been done in papers but we will try to analyze it. Some of the calculations are presented in [10] which was used as reference[1].

We have not found any reference which clearly states that the chaos exponent is also valid for the original SY of 4.2. However, it seems like this is valid and in the following section we will present an argument on why the perturbation theory of 4.2 and 4.3 are the same.

4.1 Complex SYK relation to SY

In order to calculate the Green's functions for the SYK model we have to use perturbation theory as in Chapter 2. Observing the final Schwinger-Dyson equations that are obtained for the complex SYK model in papers, we find out that they are the same with those of SY, despite the difference between 4.1 and 4.3.

Suppose that we want to calculate:

$$G(\tau) = \frac{1}{N} \sum_{i=1}^{N} \overline{\left\langle \hat{T} c_i(\tau) c_i^\dagger(0) \right\rangle} \tag{4.4}$$

for the complex SYK, where $\langle \cdot \rangle$ denotes the thermal average and the bar denotes average in J distribution. Note that in Chapter 2 we had only thermal average, because we used the replica method to average the J distribution before calculating the perturbations. We can do the same here, but we think that it is more convenient to average after doing the perturbation.

As in the first chapter we can begin by expanding $e^{-\beta H}$. We first recall that J_{ijkl} is a random variable with zero average and as a consequence the expansion will not contain

[1] This paper presents a more complicated system which contains the complex SYK interacting with a hopping Hamiltonian. Some of the calculations are the same with our case.

odd-order terms (they will vanish when we average in J). Hence, the first non-trivial term is of second order in H:

$$\overline{\mathrm{Tr}\left[\hat{T}c_i(\tau)c_i^\dagger(0)H^2\right]} \sim \frac{J^2}{N^3}\sum_{jklm}\mathrm{Tr}\left\{\hat{T}c_i(\tau)c_i^\dagger(0)\left[c_j^\dagger c_k^\dagger c_l c_m\right](\tau_1)\left[c_j^\dagger c_k^\dagger c_l c_m\right](\tau_2)\right\}$$

where we used the antisymmetric properties of J_{ijkl} when we did the bar average:

$$\overline{J_{ijkl}J_{i'j'k'l'}} = J^2\left(\delta_{ii'}\delta_{jj'}\delta_{kk'}\delta_{ll'} + \delta_{ik'}\delta_{jl'}\delta_{ki'}\delta_{lj'}\right) \tag{4.5}$$

because of which the indices at τ_1 and τ_2 are the same. In fact we can interchange $(jk) \leftrightarrow (lm)$ but these indices are summed so we get the same result. This second order term gives only one diagram:

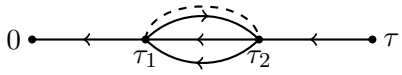

where lines denote time ordered Green's functions like 4.4 and dashed lines denote J average. The order of this diagram can be found by noting that because of 4.5, points that are connected by the dashed line carry the same indices. Therefore there are contributions of order N from each Green function that connects τ_1 with τ_2. Because of the normalization of 4.3 the total order is $N^3/N^3 = 1$ and thus the diagram contributes at $N \to +\infty$.

In fact this type of diagrams and compositions of them, referred as watermelon in [9], are the only diagrams in the self energy expansion. This way we get the equation $\Sigma(\tau) = -J^2G^2(\tau)G(-\tau)$, where $G^(\tau)$ corresponds to the two lines directed from right to left, $-G(-\tau)$ to the one from left to right and J^2 comes from the dashed average. This equation is the same as in the fermionic representation of the SY model.

As evidence that non-watermelon diagrams vanish at $N \to +\infty$ we give two possible of order H^4:

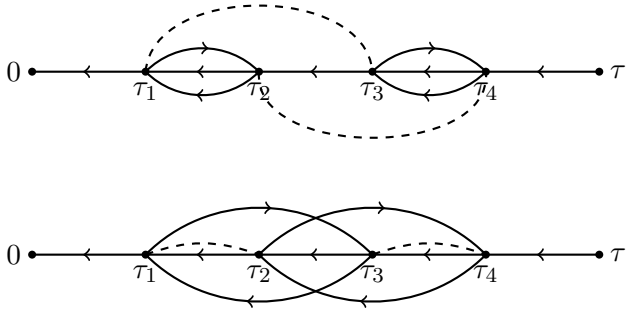

The first has order $N^3/N^6 = N^{-3}$ where each line pair of lines in the watermelons contributes N. The second has $N^4/N^6 = N^{-2}$ because we have N^2 from $\tau_2 \to \tau_1$ and $\tau_4 \to \tau_3$ and N^2 from the pairs that connect τ_1 with τ_3 and τ_2 with τ_4.

We believe that the same perturbation theory can be done for the SY model of Chapter 2. The difference there is that each c operator caries two indices, one for the site and one for the spin color, which comes from the SU(M) representation. We can correspond the pair of indices to one index of the complex SYK $(i\alpha) \leftrightarrow i$. The average $\overline{J_{ij}J_{i'j'}}$ in analogy with 4.5 will require that $(i,j) = (i',j')$ or $(i,j) = (j',i')$. On the other hand, the indices α, β will still be free and the H^2 term would look like:

$$\overline{\mathrm{Tr}\left[\hat{T}c_{00}(\tau)c^\dagger_{00}(0)H^2\right]} \sim \frac{J^2}{NM}\sum_{i,j=1}^{N}\sum_{\alpha,\beta,\gamma,\delta=1}^{M}\mathrm{Tr}\left\{\hat{T}c(\tau)c^\dagger(0)\left[c^\dagger_{i\alpha}c^\dagger_{j\beta}c_{i\beta}c_{j\alpha}\right](\tau_1)\left[c^\dagger_{i\gamma}c^\dagger_{j\delta}c_{i\delta}c_{j\gamma}\right](\tau_2)\right\}$$

The surviving watermelon diagram will have the terms:

$$\mathrm{Tr}\left[c_{00}(\tau)c^\dagger_{i\alpha}(\tau_1)\right]\mathrm{Tr}\left[c_{j\gamma}(\tau_2)c^\dagger_{j\beta}(\tau_1)\right]\mathrm{Tr}\left[c_{i\beta}(\tau_1)c^\dagger_{i\gamma}(\tau_2)\right]\mathrm{Tr}\left[c_{j\alpha}(\tau_1)c^\dagger_{j\delta}(\tau_2)\right]\mathrm{Tr}\left[c_{i\delta}(\tau_2)c^\dagger_{00}(0)\right]$$

$$\sim \delta_{i0}\delta_{\alpha 0}\delta_{jj}\delta_{\beta\gamma}\delta_{\alpha\delta}$$

and by doing the sum we find that it is of order 1. If we chose a different combination of terms (for example we did not take j's together) we would find a vanishing diagram. Therefore, the proper choice leads not only to equality of the site indices but also of the color indeces and we can see this as an equality of the total index $(i\alpha)$ and reduce the problem to the complex SYK.

4.2 Four point correlators

Before calculating the OTO correlator we analyzed in the previous chapter, we will present the calculation of the imaginary time four point correlator, because it is easier to analyze the perturbation theory in this case. We will then modify the results in order to solve the real time case. The function we would like to calculate is:

$$F(\tau_1,\tau_2,\tau_3,\tau_4) = \frac{1}{N^2}\sum_{i,j=1}^{N}\overline{\left\langle \hat{T}c^\dagger_i(\tau_1)c^\dagger_j(\tau_4)c_i(\tau_2)c_j(\tau_3)\right\rangle} \tag{4.6}$$

The route we follow is similar to the previous section and the first term is of second order in H:

$$\overline{\mathrm{Tr}\left[\hat{T}c_i^\dagger(\tau_1)c_j^\dagger(\tau_4)c_i(\tau_2)c_j(\tau_3)H^2\right]}$$

This term contains six different times, the four known and two interaction times that come from the Hamiltonian. The corresponding diagrams consist of two separate lines connecting pairs of the four known times, while the two interaction times may be either one the same or on different lines. If the two interaction times are on the same line then the diagram is called disconnected (as the two lines are separated) and it reduces to two-point Green's functions. The non trivial case is when the two lines are connected:

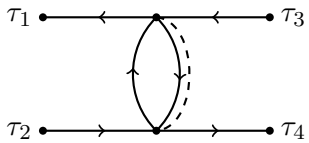

N^{-1}

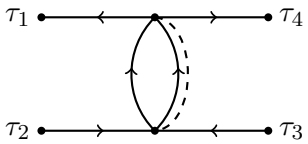

N^{-1}

As before, points connected by dashed line carry the same indices. The order of these diagrams is N^{-1}. This is valid because there is only one sum in each of the lines that connect the middle points. Therefore we have order N^2, which is divided by the N^3 of H^2 to give the final N^{-1}.

A result of this observation is that in the $N \to +\infty$ limit connected diagrams do not contribute to the four point diagrams and the problem reduces to disconnected diagrams which are Green's functions. We used this result in Chapter 2 to argue that $Q(\tau) = G(\tau)G(-\tau)$.

However, chaos is apparent in the N^{-1} terms of the expansion and thus here we need to take into account these connected diagrams. In fact, since the order 1 terms are trivial Green functions we only need to calculate only the N^{-1} term which will be denoted by $\mathcal{F}$. If we proceed to the next order (fourth) we find superpositions of these diagrams. These are referred as ladder in [9] are all of order N^{-1} and contribute to $\mathcal{F}$. In the fourth order we also have other diagrams like:

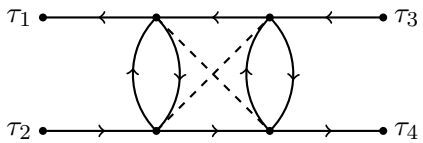

but these have order less than N^{-1} and do not contribute. It is apparent that if we continue to higher orders of H, only ladder diagrams survive.

Notice that the arrows' directions are important in this case. The rules for finding this direction is: First, fermions leave from τ_2 and τ_4 and go to τ_1 and τ_3 because of the creation and annihilation operators in definition 4.6. Also, in every other point the number of fermions that go into must be same with the number of those that leave.

The direction is important because the model has complex fermions and makes the perturbations slightly more complicated than the Majorana fermion model in [9]. If we sum the ladder diagrams we will find two different series which corresponds to the two different diagrams of the second order. Diagrammatically:

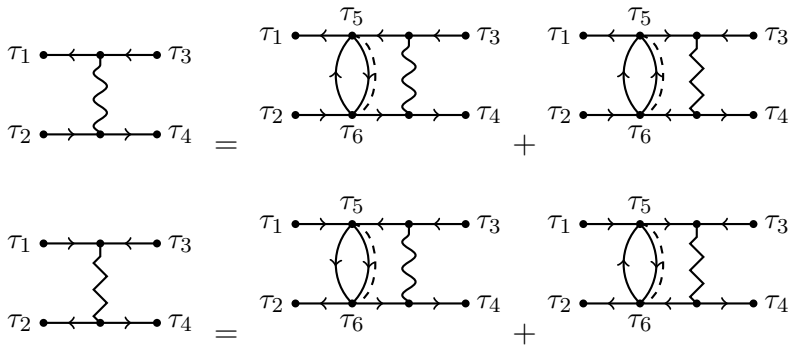

where the wavelike line is $\mathcal{F}(\tau_1, \tau_2, \tau_3, \tau_4)$ while the zigzag line is $\mathcal{F}(\tau_2, \tau_1, \tau_3, \tau_4)$. This is different from previous self-consistency diagrammatic equations we had in this work because it involves a coupling between these two different functions. We understand that the equation will have the form:

$$\begin{pmatrix} \mathcal{F}(\tau_1, \tau_2, \tau_3, \tau_4) \\ \mathcal{F}(\tau_2, \tau_1, \tau_3, \tau_4) \end{pmatrix} = \int_{-\infty}^{+\infty} \int_{-\infty}^{+\infty} \mathbf{K}(\tau_1, \tau_2, \tau_5, \tau_6) \begin{pmatrix} \mathcal{F}(\tau_5, \tau_6, \tau_3, \tau_4) \\ \mathcal{F}(\tau_6, \tau_5, \tau_3, \tau_4) \end{pmatrix} d\tau_5 d\tau_6 \tag{4.7}$$

and we can find the kernel from the diagrams. Because of the coupling, we have to be cautious with the combinatorial coefficients which we ignored until now. The first diagram contains the terms:

$$\left\langle c_i^\dagger(\tau_1) c_3(\tau_5) \right\rangle \left\langle c_i(\tau_2) c_1^\dagger(\tau_6) \right\rangle \left\langle c_j(\tau_3) c_1^\dagger(\tau_5) \right\rangle \left\langle c_i^\dagger(\tau_4) c_3(\tau_6) \right\rangle ...$$

where the indices $1, .., 4$ are abbreviation for $i_1, ...i_4$. Here 3 and 1 in the first to terms were chosen arbitrarily and there are 4 combinations from this. Once these two are chosen we have two choices for the $c_j(\tau_3)$ pair, either $c_1^\dagger(\tau_5)$ or $c_2^\dagger(\tau_5)$ as we haven't used any of these before and we need to go to τ_5 point. On the contrary, the second diagram can start

with one of the 4 combination but has to continue as:

$$\left\langle c_j(\tau_3)c_2^\dagger(\tau_6)\right\rangle \left\langle c_i^\dagger(\tau_4)c_3(\tau_6)\right\rangle ...$$

because we have to connect $c_j(\tau_3)$ with τ_6. This leaves us one option because we have used the other τ_6 creation operator in one of the fist two terms. According to this reasoning we have to double the diagonal elements of the kernel:

$$\mathbf{K}(\tau_1,\tau_2,\tau_3,\tau_4) = J^2 \begin{pmatrix} 2G(\tau_{31})G(\tau_{24})G(\tau_{34})G(\tau_{43}) & -G(\tau_{31})G(\tau_{24})G^2(\tau_{43}) \\ -G(\tau_{13})G(\tau_{42})G^2(\tau_{34}) & 2G(\tau_{13})G(\tau_{42})G(\tau_{34})G(\tau_{43}) \end{pmatrix} \tag{4.8}$$

where $\tau_{nm} = \tau_n - \tau_m$. The minus sign comes, as always, because of the time ordering of Grassmann variables. Equations 4.7 and 4.8 give the $1/N$ element in the expansion of the real time four point correlator in the limit $N \to +\infty$.

4.3 Out-of-time-ordered correlators

The main purpose of the perturbation theory of the previous section is the calculation of the OTO correlators introduced in Chapter 3, as a quantity that indicates chaos if it has a specific behavior. The regularized OTO correlators for our system are [10]:

$$\begin{aligned} F_1(t_1,t_2) &= \frac{1}{N^2}\sum_{i,j=1}^{N} \overline{\mathrm{Tr}\left[yc_i^\dagger(t_1)yc_j^\dagger(0)yc_i(t_2)yc_j(0)\right]} \\ F_2(t_1,t_2) &= \frac{1}{N^2}\sum_{i,j=1}^{N} \overline{\mathrm{Tr}\left[yc_i(t_1)yc_j^\dagger(0)yc_i^\dagger(t_2)yc_j(0)\right]} \end{aligned} \tag{4.9}$$

where $y^4 = e^{-\beta H}$. The need to define two such functions is related to coupling between two different functions in 4.7.

Diagrammatic perturbation theory for the OTOC is the same with the previous section. However, we have to beware that 4.9 is in real time and we do not have the time-ordering symbol. The action of this symbol is crucial when deriving mathematical equations from the corresponding diagrams. An easy solution for the current problem is to use the Keldysh formalism in order to write the OTOCs as time ordered correlators in a contour in the complex plane [7][10][27]. After doing this we can use the diagrams of the previous section to derive kinetic equations.

The Keldysh formalism and the analytic continuation in real time changes the imaginary time Green's functions appearing in 4.8. Specifically $G(\tau_{31}) \to G^A(t_{31})$ and $G(\tau_{24}) \to G^R(t_{24})$ where the advanced and retarded Green's functions were introduced in Appendix B. We also introduce the Wightmann correlator:

$$G^{\pm}_{lr}(t) = iG\left(\tau \to it \pm \frac{\beta}{2}\right) \tag{4.10}$$

and $G(\tau_{24}) \to G^{+}_{lr}(t_{24})$, $G(\tau_{42}) \to G^{-}_{lr}(t_{42})$. Using these, the kinetic equations 4.7 and 4.8 are written as:

$$\begin{pmatrix} \mathcal{F}_1(t_1,t_2) \\ \mathcal{F}_2(t_1,t_2) \end{pmatrix} = \int_{-\infty}^{+\infty}\int_{-\infty}^{+\infty} \mathbf{K}(t_1,t_2,t_3,t_4) \begin{pmatrix} \mathcal{F}_1(t_3,t_4) \\ \mathcal{F}_2(t_3,t_4) \end{pmatrix} dt_3 dt_4 \tag{4.11}$$

$$\mathbf{K}(t_1,t_2,t_3,t_4) = J^2 \begin{pmatrix} 2G^A(t_{31})G^R(t_{24})G^{+}_{lr}(t_{43})G^{-}_{lr}(t_{34}) & -G^A(t_{31})G^R(t_{24})\left[G^{+}_{lr}(t_{43})\right]^2 \\ -G^R(t_{13})G^A(t_{42})\left[G^{-}_{lr}(t_{34})\right]^2 & 2G^R(t_{13})G^A(t_{42})G^{+}_{lr}(t_{43})G^{-}_{lr}(t_{34}) \end{pmatrix} \tag{4.12}$$

4.4 Kernel evaluation

In section 2.9 we found the Green's functions for the SY model in non-zero temperature. For simplicity in symbolism we substitute $\theta + \frac{\pi}{4} \to \theta$ and from 2.47 we have:

$$G(\tau) = \frac{Ae^{-a\tau/\beta}}{\left(\beta J \sin\frac{\pi|\tau|}{\beta}\right)^{1/2}} \begin{cases} -\sin\theta & ,\tau > 0 \\ \cos\theta & ,\tau < 0 \end{cases} \tag{4.13}$$

with $A = (\pi/J^2 \sin 2\theta)^{1/4}$. We can use B.8 to continue these results to real time:

$$G^R(t) = i\Theta(t)\left[\frac{Ae^{-iat/\beta}(-\sin\theta)}{\left(i\beta J \sinh\frac{\pi t}{\beta}\right)^{1/2}} - \frac{Ae^{-iat/\beta}\cos\theta}{\left(-i\beta J \sinh\frac{\pi t}{\beta}\right)^{1/2}}\right] \Rightarrow$$

$$\Rightarrow G^R(t) = -\Theta(t)\frac{Ae^{-iat/\beta}e^{i\theta}}{\left(i\beta J \sinh\frac{\pi t}{\beta}\right)^{1/2}} \tag{4.14}$$

and:

$$G^A(t) = \Theta(-t)\frac{Ae^{-iat/\beta}e^{-i\theta}}{\left(i\beta J \sinh\frac{\pi t}{\beta}\right)^{1/2}} \tag{4.15}$$

Similarly, Wightmann correlators 4.10 are:

$$G^{+}_{lr}(t) = -\frac{Ae^{-iat/\beta}e^{-a/2}}{\left(\beta J \cosh\frac{\pi t}{\beta}\right)^{1/2}}\sin\theta \tag{4.16}$$

$$G^{-}_{lr}(t) = \frac{Ae^{-iat/\beta}e^{a/2}}{\left(\beta J \cosh\frac{\pi t}{\beta}\right)^{1/2}}\cos\theta \tag{4.17}$$

The first element of the kernel 4.12 will be:

$$2J^2 G^A(t_{31})G^R(t_{24})G^{+}_{lr}(t_{43})G^{-}_{lr}(t_{34}) = \Theta(t_{13})\Theta(t_{24})\frac{A^4 e^{-ia(t_{31}+t_{24}+t_{34}+t_{43})/\beta}}{\beta^2\left(-\sinh\frac{\pi t_{31}}{\beta}\sinh\frac{\pi t_{24}}{\beta}\right)^{1/2}\cosh\frac{\pi t_{34}}{\beta}}\sin 2\theta =$$

$$= \frac{\pi\Theta(t_{13})\Theta(t_{24})e^{ia(t_{12}-t_{34})/\beta}}{\beta^2\left(\sinh\frac{\pi t_{13}}{\beta}\sinh\frac{\pi t_{24}}{\beta}\right)^{1/2}\cosh\frac{\pi t_{34}}{\beta}}$$

where we used A value and that $t_{13} - t_{24} = t_1 - t_3 - t_2 + t_4 = t_{12} - t_{34}$. The rest of the elemnents can be calculated similarly and the total kernel is:

$$\mathbf{K}(t_1,t_2,t_3,t_4) = \frac{\pi}{\beta^2}K\begin{pmatrix} e^{ia(t_{12}-t_{34})/\beta} & \frac{1}{2}\tan\theta e^{ia(t_{12}+t_{34})/\beta} \\ \frac{1}{2}\cot\theta e^{-ia(t_{12}+t_{34})/\beta} & e^{-ia(t_{12}-t_{34})/\beta}\end{pmatrix} \tag{4.18}$$

where

$$K(t_1,t_2,t_3,t_4) = \frac{\Theta(t_{13})\Theta(t_{24})}{\left(\sinh\frac{\pi t_{13}}{\beta}\sinh\frac{\pi t_{24}}{\beta}\right)^{1/2}\cosh\frac{\pi t_{34}}{\beta}} \tag{4.19}$$

We note that the diagonal elements of the kernel do not have θ dependence and if we assume that this procedure is valid for the SY model then this means that they are independent of total spin (θ measures total spin in the SY). On the other hand, the non-diagonal coupling terms are theta dependent because we have $(G^{\pm}_{lr})^2/\sin 2\theta \sim (\tan\theta)^{\pm 1}$. Also, θ makes the kernel non-Hermitian: The kernel is Hermitian only for $\theta = \pi/4$ which according to Luttinger relation 2.40 corresponds to $q_0 = 1/2$ the middle of $0 \leq q_0 \leq 1$.

Since kinetic equations 4.11 contain integrals in t_3, t_4, it would be useful to separate these variables from t_1, t_2. This can be done by defining:

$$\mathbf{T}(t) = \begin{pmatrix} e^{-iat}\cot\theta & 0 \\ 0 & e^{iat}\end{pmatrix} \tag{4.20}$$

and observing that 4.18 can be written as:

$$\mathbf{K}(t_1,t_2,t_3,t_4) = \frac{\pi}{\beta^2} K \mathbf{T}^{-1}(t_{12}) \left(\mathbf{I} + \frac{\sigma_1}{2}\right) \mathbf{T}(t_{34}) \tag{4.21}$$

where σ_1 is the x-axis Pauli matrix.

4.5 Solving the kinetic equations

Knowing the exact form of the kernel, we can attempt to solve equation 4.11. Defining:

$$|\mathcal{F}(t_1,t_2)\rangle = \mathbf{T}(t_1-t_2) \begin{pmatrix} \mathcal{F}_1(t_1,t_2) \\ \mathcal{F}_2(t_1,t_2) \end{pmatrix} \tag{4.22}$$

we have to solve:

$$|\mathcal{F}(t_1,t_2)\rangle = \frac{\pi}{\beta^2}\left(\mathbf{I} + \frac{\sigma_1}{2}\right) \int_{-\infty}^{+\infty}\int_{-\infty}^{+\infty} K(t_1,t_2,t_3,t_4)\,|\mathcal{F}(t_3,t_4)\rangle\, dt_3 dt_4 \tag{4.23}$$

which can be transformed into a scalar equation if we use the eigenvectors of σ_1:

$$\mathcal{X}(t_1,t_2) = \frac{\pi}{\beta^2} k \int_{-\infty}^{+\infty}\int_{-\infty}^{+\infty} K(t_1,t_2,t_3,t_4)\mathcal{X}(t_3,t_4) dt_3 dt_4 \tag{4.24}$$

where $k = 1/2$ or $k = 3/2$. We change the variables to $t = \pi(t_1+t_2)/(2\beta)$ and $s = \pi t_{12}/(2\beta)$ and similarly t', s' for t_3, t_4. Using the kernel 4.19 we write last equation as:

$$X(t,s) = \frac{2k}{\pi}\int_{-\infty}^{+\infty}\int_{-\infty}^{+\infty} \frac{\Theta(t-t'+s-s')\Theta(t-t'-s+s')}{(\sinh(t-t'+s-s')\sinh(t-t'-s+s'))^{1/2}} \frac{X(t',s')}{\cosh s'} dt ds =$$

$$= \frac{2k}{\pi}\int_{-\infty}^{+\infty}\int_{-\infty}^{+\infty} \frac{\Theta(x+y)\Theta(x-y)}{(\sinh(x+y)\sinh(x-y))^{1/2}} \frac{X(t-x,s-y)}{\cosh(s-y)} dx dy$$

where:

$$X(t,s) = \mathcal{X}\left(\frac{\beta}{\pi}(t+s), \frac{\beta}{\pi}(t-s)\right) \tag{4.25}$$

Following [8][9][10] we use the ansatz $X(t,s) = e^{\mu t} f(s)$. This form must be a solution if the model is chaotic. The Lyapunov exponent is related to μ by $\mathcal{X}(t_1,t_2) \sim e^{\lambda_L(t_1+t_2)/2}$ which according to 4.25 means that $\lambda_L = \mu\pi/\beta$. The equation is:

$$f(s) = \frac{1}{\pi}\int_{-\infty}^{+\infty} F(y)\frac{f(s-y)}{\cosh(s-y)} dy = \frac{1}{\pi}\int_{-\infty}^{+\infty} F(s-y)\frac{f(y)}{\cosh y} dy \tag{4.26}$$

where:

$$F(y) = 2k \int_{-\infty}^{+\infty} \frac{e^{-\mu x}\Theta(x+y)\Theta(x-y)}{(\sinh(x+y)\sinh(x-y))^{1/2}} dx \tag{4.27}$$

Since 4.26 is a convolution we can use Fourier transform to make it a product in frequencies:

$$\tilde{f}(\omega) = \frac{\tilde{F}(\omega)}{2\pi} \int_{-\infty}^{+\infty} \frac{\tilde{f}(\omega')d\omega'}{\cosh \pi(\omega - \omega')} \tag{4.28}$$

where we used the Fourier transform of $(\cosh y)^{-1}$ which is $\sim (\cosh \pi\omega)^{-1}$. The Fourier transform of F can be calculated by defining $L(x) = \Theta(x)/\sqrt{\sinh(x)}$ and writing:

$$F(y) = 2k \int_{-\infty}^{+\infty} e^{-\mu x} L(x+y)L(x-y)dx$$

which transforms as:

$$\tilde{F}(\omega) = 2k \int \exp i\left[\omega y - \omega_1(x+y) - \omega_2(x-y) + i\mu x\right] \tilde{L}(\omega_1)\tilde{L}(\omega_2)\frac{d\omega_1 d\omega_2}{4\pi^2}dxdy \Rightarrow$$

$$\Rightarrow \tilde{F}(\omega) = 2k\tilde{L}\left(i\mu + \omega\right)\tilde{L}\left(i\mu - \omega\right)$$

We can then use the Fourier transform of L:

$$\int_{-\infty}^{+\infty} \frac{\Theta(x)}{\sqrt{\sinh(x)}} e^{i\omega x} dx = \sqrt{\frac{\pi}{2}} \frac{\Gamma\left(\frac{1}{4} - i\omega\right)}{\Gamma\left(\frac{3}{4} - i\omega\right)}$$

to get:

$$\tilde{F}(\omega) = \pi k \left| \frac{\Gamma\left(\frac{1}{4} + \frac{\mu}{2} + i\omega\right)}{\Gamma\left(\frac{3}{4} + \frac{\mu}{2} + i\omega\right)} \right|^2$$

where the conjugate property $\Gamma^*(z) = \Gamma(z^*)$ was used. If we use this and Euler's reflection formula to write cosh as a Γ function, we can write 4.28 in the form of [9][10]:

$$\tilde{f}(\omega) = \frac{k}{2\pi} \left| \frac{\Gamma\left(\frac{1}{4} + \frac{\mu}{2} + i\omega\right)}{\Gamma\left(\frac{3}{4} + \frac{\mu}{2} + i\omega\right)} \right|^2 \int_{-\infty}^{+\infty} \left| \Gamma\left(\frac{1}{2} + i(\omega - \omega')\right) \right|^2 \tilde{f}(\omega')d\omega' \tag{4.29}$$

This is an eigenfunction equation for f. In fact we are mostly interested in the eigenvalues which will give us the value of the Lyapunov exponent μ. We have not found a way to solve this problem in general. A solution that follows from some properties of Γ function and is given in papers is:

$$\tilde{f}(\omega) = \left| \Gamma\left(\frac{1}{4} + \frac{\mu}{2} + i\omega\right) \right|^2 \tag{4.30}$$

If we insert this in 4.29 we get the equation for μ:

$$\Gamma\left(\frac{3}{2}+\mu\right) = k\Gamma\left(\frac{1}{2}+\mu\right) \Rightarrow \mu = k - \frac{1}{2} \tag{4.31}$$

Recalling that k represents the eigenvalues of the matrix $\mathbf{I}+\sigma_1/2$ which are $k = 1/2, 3/2$, the possible values are $\mu = 0, 1$. We also recall that the ansatz was $\mathcal{X} \sim e^{\lambda_L(t_1+t_2)/2}$ with $\lambda_{\mathrm{L}} = 2\mu\pi/\beta$, so the solution $\mu = 1$ survives in large times, which corresponds to $\lambda_{\mathrm{L}} = 2\pi T$. Hence, the model saturates the Lyapunov exponent bound proposed in [15].

Someone might argue that 4.30 might not be a unique solution of 4.29 and that other eigenfunctions might exist that allow different values of μ. If we accept the Lyapunov exponent bound, then even if other μ values exist, they will be smaller (or equal) than $\lambda_{\mathrm{L}} = 2\pi T$ and they will not contribute at large times.

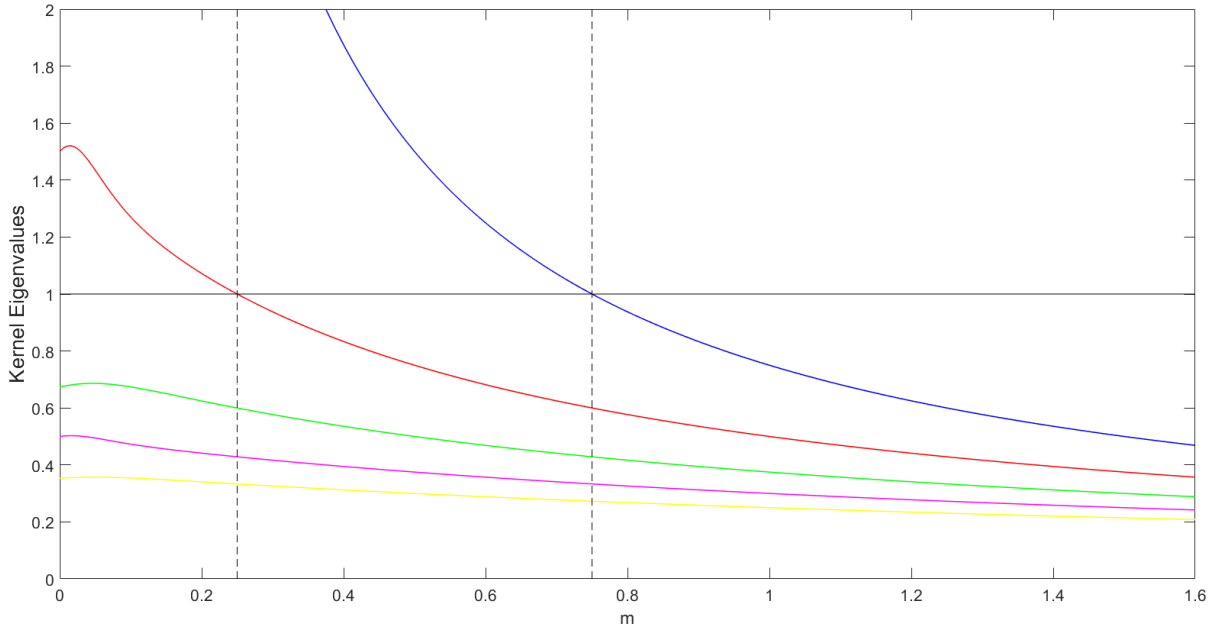

FIGURE 4.1: Four larger eigenvalues of the integral kernel for $k = 3/2$. We find that 1 is an eigenvalue only if $m \equiv (1+2\mu)/4$ equals 0.25 or 0.75. The latter is the saturation of the bound and we have no greater solutions as the larger eigenvalue (blue) is clearly smaller than 1.

Even if we do not accept the bound, we can provide a numerical argument that no values larger than $\mu = 2$ exist. For this, we take the discrete limit of 4.29 where the integral becomes a matrix eigenvalue problem and find the values of μ for which we have an eigenvalue of unity. In Appendix D we give the code that does this and in Figure 4.1 we plot the five largest eigenvalues for $k = 3/2$. The dashed lines give the two values of

$m \equiv (1+2\mu)/4$ for which 1 is an eigenvalue. These values are $m = 0.25, 0.75$ which give $\mu = 0, 1$. The same figure for $k = 1/2$ gives only $\mu = 0$. Therefore we confirmed that $\mu = 1 \Rightarrow \lambda_{\mathrm{L}} = 2\pi T$ is the dominating eigenvalue in any case.

4.6 Summary of results

The analysis of this chapter showed that the complex SYK model, as its Majorana counterpart, saturates the chaos bound proposed in [15]. The Lyapunov exponent is found from the increasing $1/N$ part of the OTO correlators, which leads to a decrease in the total OTO correlator and implies fast scrambling of information. In [15] it is conjectured that the systems that saturate the bound have a gravity dual, so it is believed that this is true for SYK.

Chaos arguments are a serious indication of the correspondence between SYK and gravity, but not the only indication. A source of the model's properties is a reparametrization symmetry (the conformal symmetry) which exists at low frequencies and breaks at higher. According to [9], this pattern also exists in near extremal black holes and hence is the motivation to study SYK as a holographic model. According to the same work, this symmetry is the reason for the system's futures, like its chaotic behavior. They believe that these effects may appear in other condensed matter systems as well.

Appendix A

Diagrammatic Perturbation Theory

In this appendix we give the details of the diagrammatic perturbation theory through which we find Schwinger-Dyson equations BOS1-BOS3 and FER1-FER3. We will present this only for the bosonic case as the fermionic is similar.

The main idea is to treat the interaction defined by the functional 2.17 as a perturbation to free particle Hamiltonian. We expand this perturbation in orders of $1/M$ and we hope that for $M \to +\infty$ the expansion is simplified in a way that we can sum the remaining terms and acquire a recursive relation for G.

We write the functional 2.17 in the bosonic representation:

$$\mathcal{L}[b, b^\dagger] = \frac{J^2}{2M} \sum_{c,d=1}^{n} \int_0^\beta \int_0^\beta Q^{cd}(\tau - \tau') b_\mu^{c\dagger}(\tau_1) b_\nu^c(\tau_1) b_\nu^{d\dagger}(\tau_2) b_\mu^d(\tau_2) d\tau_1 d\tau_2 \tag{A.1}$$

Repeated greek subscripts are summed. We define the free particle Green's function:

$$G_0^{ab}(\tau) = \frac{1}{M} \left\langle T b_\mu^a(\tau) b_\mu^{b\dagger}(0) \right\rangle_0 \tag{A.2}$$

Here the thermal average caries the subscript 0 because it is taken in repsect to a free particle Hamiltonian:

$$\mathcal{L}_0[b, b^\dagger] = \sum_\mu \int_0^\beta b_\mu^\dagger (\partial_\tau - \lambda) b_\mu d\tau \tag{A.3}$$

There the dagger is used as a symbol for complex conjugate, as after the transformation to path integral b are numbers, not operators. The chemical potential λ is introduced

because of the constraint:

$$G^{aa}(\tau = 0^-) = \frac{1}{M} \left\langle b_\mu^{a\dagger}(0) b_\mu^a(0^-) \right\rangle = \kappa \tag{A.4}$$

Equation A.2 gives the Green's function of a free particle which can be easily calculated and its Fourier transform is:

$$(G_0^{-1})^{ab}(i\omega_n) = -i\omega_n + \lambda \tag{A.5}$$

where $\omega_n = 2n\pi/\beta$, $n \in \mathbb{Z}$ the bosonic Matsubara frequencies.

We want an expression of the full Green's function $G^{ab}(\tau)$ in terms of $G_0^{ab}(\tau)$. We start with:

$$G_B^{ab}(\tau) = \frac{\left\langle T b_\mu^a(\tau) b_\mu^{b\dagger}(0) e^{\mathcal{L}} \right\rangle_0}{M \left\langle T e^{\mathcal{L}} \right\rangle_0}$$

where $\mathcal{L}$ is given by A.1. If we expand the exponential in its Taylor series we find that the first orders of $\mathcal{L}$ are:

$$\frac{\left\langle F(b) e^{\mathcal{L}} \right\rangle}{\left\langle e^{\mathcal{L}} \right\rangle} = \langle F \rangle + \langle F\mathcal{L} \rangle - \langle F \rangle \langle \mathcal{L} \rangle + \tag{A.6}$$

$$+\frac{1}{2} \left(\left\langle F\mathcal{L}^2 \right\rangle - \langle F \rangle \left\langle \mathcal{L}^2 \right\rangle \right) - \left(\langle F\mathcal{L} \rangle \langle \mathcal{L} \rangle - \langle F \rangle \langle \mathcal{L} \rangle^2 \right) + \mathcal{O}(\mathcal{L}^3)$$

The free particle Hamiltonian A.3 is diagonal in b and we can use Wick's theorem to reduce the averages in two point functions which can be expressed in terms of G_0. As an example we give the first order term:

$$\langle F\mathcal{L} \rangle \sim \frac{1}{M} \left\langle T b_\mu^a(\tau) b_\mu^{b\dagger}(0) b_\sigma^{c\dagger}(\tau_1) b_\tau^c(\tau_1) b_\tau^{d\dagger}(\tau_2) b_\sigma^d(\tau_2) \right\rangle$$

which gives the terms:

$$\left\langle b_\mu^a(\tau) b_\mu^{b\dagger}(0) \right\rangle \left\langle T b_\sigma^{c\dagger}(\tau_1) b_\tau^c(\tau_1) b_\tau^{d\dagger}(\tau_2) b_\sigma^d(\tau_2) \right\rangle$$

$$\left\langle b_\mu^a(\tau) b_\sigma^{c\dagger}(\tau_1) \right\rangle \left\langle b_\tau^c(\tau_1) b_\mu^{a\dagger}(0) \right\rangle \left\langle b_\tau^{d\dagger}(\tau_2) b_\sigma^d(\tau_2) \right\rangle$$

$$\left\langle b_\mu^a(\tau) b_\sigma^{c\dagger}(\tau_1) \right\rangle \left\langle b_\sigma^d(\tau_2) b_\mu^{a\dagger}(0) \right\rangle \left\langle T b_\tau^{d\dagger}(\tau_2) b_\tau^c(\tau_1) \right\rangle$$

To be more exact, this analysis gives more terms than these three. In fact, the total pairs of the six 'operators' are 15, however, only the pairs that contain both a b and a $b^\dagger$ survive and even some of them are the same. For example, for the first pair we can

choose $b^a_\mu(\tau)$ with either $b^{c\dagger}_\sigma(\tau_1)$ or $b^{d\dagger}_\tau(\tau_2)$ without altering the result (there is nothing that distinguishes τ_1 and τ_2 for the first choice). Mathematically we can prove this by interchanging the names of the dummy indeces. These pairs that appear more than once, result to numerical coefficients that multiply each term. It will become apparent that it is not necessary to evaluate these coefficients.

We also notice that the first term of the three distinguishes $\mathcal{L}$. It is obvious from the expansion A.6 that such terms cancel with the expansion of the denominator $\langle e^{\mathcal{L}} \rangle_0$.

Due to the diagonality of A.3, it is:

$$\left\langle T b^a_\mu(\tau) b^{b\dagger}_\nu(\tau') \right\rangle = G^{ab}_0(\tau - \tau')\delta_{\mu\nu}$$

Note that this reproduces the definition A.2 in the case $\mu = \nu$ as $\delta_{\mu\mu} = \mathrm{Tr}\, 1 = M$. Using this result we can write the two first order terms that we found as:

$$G^{ac}_0(\tau - \tau_1)\delta_{\mu\sigma} G^{cb}_0(\tau_1 - 0)\delta_{\mu\tau} G^{dd}_0(\tau_2 - \tau_2)\delta_{\tau\sigma} \sim M$$

$$G^{ac}_0(\tau - \tau_1)\delta_{\mu\sigma} G^{db}_0(\tau_2 - 0)\delta_{\mu\sigma} G^{dd}_0(\tau_2 - \tau_2)\delta_{\tau\tau} \sim M^2$$

where we found the order of M by doing the δ-summations and taking into account that G_0 is of order 1 (see for example A.4). Remembering that this terms are divided by M^2, because of the definition of G and the coefficient of $\mathcal{L}$ in A.1, we see that the first term contributes in order M^{-1} while the second in order 1. This means that in the limit $M \to \infty$, only the second order contributes.

We need to evaluate similar terms in all orders of $\mathcal{L}$. The most convenient way to do so is by drawing a diagram for each term. We use a normal line in place of G_0 and a dotted line in place of the interaction:

$$J^2 \sum_{c,d=1}^{n} \int_0^\beta \int_0^\beta Q^{cd}(\tau - \tau') \bullet d\tau_1 d\tau_2$$

that comes from A.1. Each point of the diagramms corresponds to a specific imaginary time τ. Thus the diagramms for the two first order terms are:

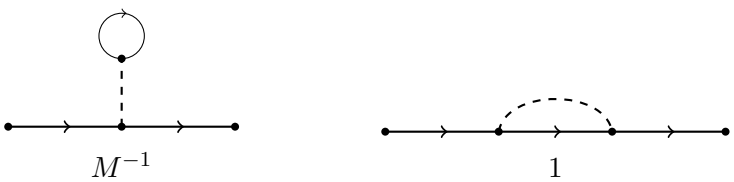

where we wrote the corresponding order of M bellow each one.

The benefit of the diagrams is that we can find all the terms of all orders without writing the corresponding equations. We always start from the point $\tau = 0$ and end at τ making all the possible connections between the times $\tau_1, \tau_2, ...$ that we integrate out. For the n-th order of $\mathcal{L}$ we have $\tau_1, \tau_2, ...\tau_{2n}$ and n dashed lines. For example, the second order diagrams are:

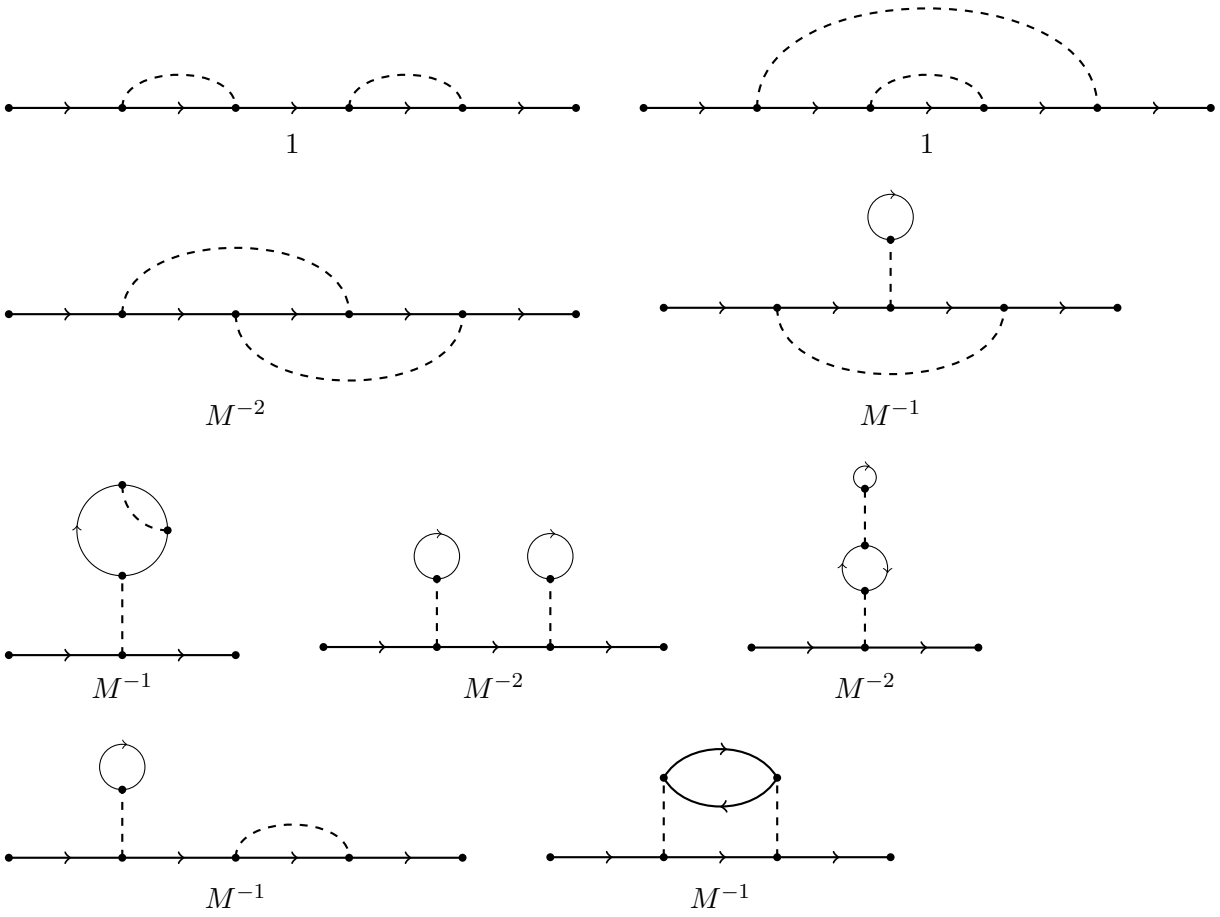

The order of M of each diagram can be evaluated by writing the δ indices that correspond to each point. Points that are connected by a dashed line carry the same pair of indices. For example, the second diagram in the first line has $\delta_{\mu\sigma_1}\delta_{\sigma_2\sigma_3}\delta_{\sigma_4\sigma_4}\delta_{\sigma_3\sigma_2}\delta_{\sigma_1\mu} = M^3$ and divided by M^3 (because it is of order $\mathcal{L}^2$) has order 1.

We observe that the only second order diagrams that survive the $M \to \infty$ limit are the two in the first line. This is easily generalized in high order diagrams and we conclude that in this limit, the exact expansion of G_B is:

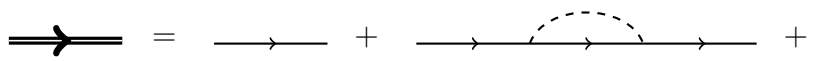

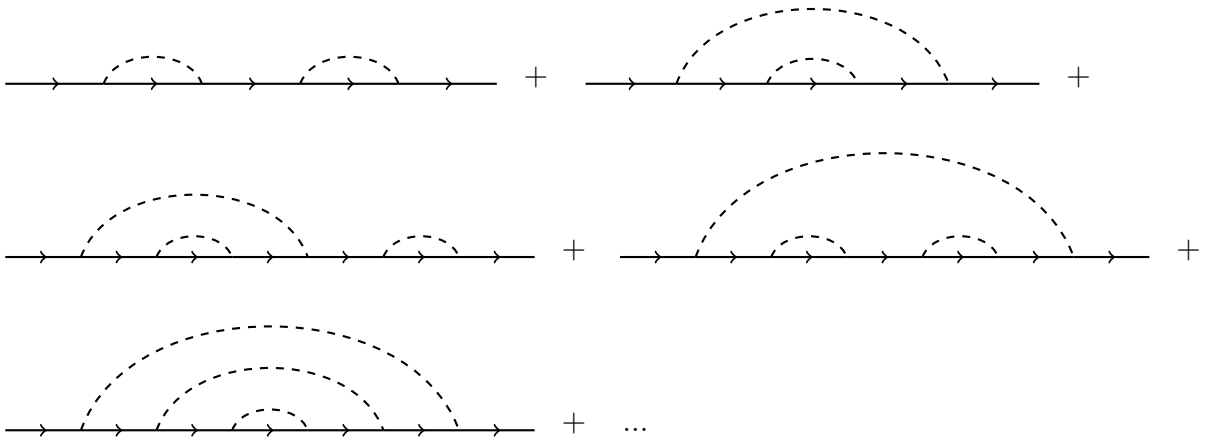

where the bold line corresponds to G_B. In fact, the problem is solvable in the limit $M \to \infty$ because we can neglect the rest of the diagrams (this is called the non-crossing approximation).

The summation of the surviving diagrams can be done using Dyson's self-energy. We observe that if a diagram like:

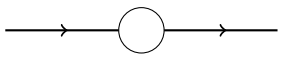

is included in the series then all the diagrams:

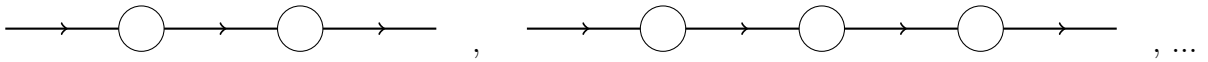

are included as well. As a result we can define the self energy as the sum of all one-particle irreducible diagrams, namely those that contain only one part:

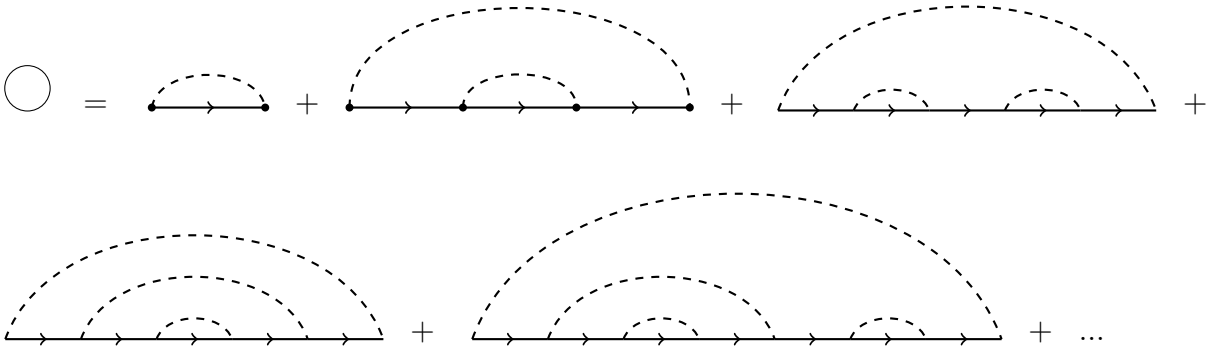

and the series for G_B becomes:

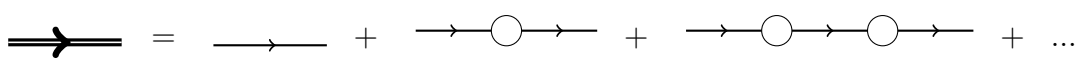

which gives the recurrence relation:

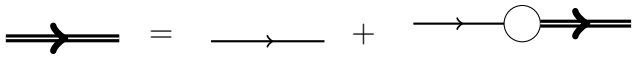

Consequently G_B is evaluated if we evaluate the self energy operator. If we recall that the dashed line represents a sum and an integral, we understand that we can erase the outer dashed line from each diagram in the self-energy series and bring it back after we do the summation. The summation, after erasing the outer dashed line, is identical to the series for  , therefore the recurrence relation is:

At this point it should be obvious why the combinatorial coefficients that multiply each diagram do not affect the result. We are only interested in the Dyson's equation which is this last relation. The coefficients are hidden in the sum of the self energy which we replaced by the sum for G_B. The only thing that matters is that these two sums are identical, not their exact formula.

Recalling the meaning of each symbol, we can write this relation mathematically as:

$$G_B^{ab}(\tau) = G_0^{ab}(\tau) + \sum_{c,d=1}^{n} \int_0^\beta \int_0^\beta G_0^{ac}(\tau_1)\Sigma_B^{cd}(\tau_2 - \tau_1)G_B^{db}(\tau - \tau_2)d\tau_1 d\tau_2 \tag{A.7}$$

where

$$\Sigma_B^{ab}(\tau) = J^2 Q^{ab}(\tau)G_B^{ab}(\tau) \tag{A.8}$$

is the operator related to self energy. Using the Fourier series of 2.20, we write A.7 as:

$$G_B^{ab}(i\omega_n) = G_0^{ab}(i\omega_n) + \sum_{c,d=1}^{n} G_0^{ac}(i\omega_n)\Sigma_B^{cd}(i\omega_n)G_B^{db}(i\omega_n) \tag{A.9}$$

The sum in replicas can be thought as matrix multiplication and the equation takes the form $G = G_0 + G_0\Sigma G$, which is a Dyson's equation. Successive applications of this give:

$$(G_B^{-1})^{ab}(i\omega_n) = (i\omega_n + \lambda)\delta^{ab} - \Sigma_B^{ab}(i\omega_n) \tag{A.10}$$

where we used A.5 for G_0^{-1}. In order to complete this equation we have to express self-energy in terms of G_B. This is straightforward combining A.8 with 2.16. The average of 2.16 is:

$$Q^{ab}(\tau) = \frac{1}{M^2}\left\langle T b_\mu^{a\dagger}(\tau) b_\nu^a(\tau) b_\nu^{b\dagger}(0) b_\mu^b(0)\right\rangle \tag{A.11}$$

which can be calculated perturbatively as before. Here we have to different lines going from 0 to τ, which may or may not interact. Drawing the diagrams for the low orders of $\mathcal{L}$ we can see that the diagrams where there is interaction (dashed line) that connects the two lines do not survive the $M \to \infty$ limit. Hence we sum the diagrams where the two lines are independent and we get one $G_B(\tau)$ for each line, that is $Q^{ab}(\tau) = G_B^{ab}(\tau)G_B^{ba}(-\tau)$. The minus sign exists because the μ sum in A.11 starts with $b^\dagger$ instead of b. The self-energy is given by A.8:

$$\Sigma_B^{ab}(\tau) = J^2 \left[G_B^{ab}(\tau)\right]^2 G_B^{ba}(-\tau) \tag{A.12}$$

The Green's function for the bosonic case is the solution of equations A.10 and A.12.

The main difference in the fermionic model is that the f operators in different replicas anticommute, in contrast to b operators that commute. This anticommutanion introduces some minus signs in diagramms where we have to flip operators because of the time ordering. This signs are the same in both the G_F and Σ_F expansions, so we expect the Dyson's equation A.9 to be the same with the bosonic case. Consequently, A.10 is valid for the fermionic case.

On the other hand, there is a difference in the calculation of Q^{ab}. As we analysed in the bosonic case, in this calculation we have to change one $G_B^{ab}(\tau) \to G_B^{ba}(-\tau)$. The corresponding change in the fermions gives a minus sign: $G_F^{ab}(\tau) \to -G_F^{ba}(-\tau)$ and as a result A.12 becomes:

$$\Sigma_F^{ab}(\tau) = -J^2 \left[G_F^{ab}(\tau)\right]^2 G_F^{ba}(-\tau) \tag{A.13}$$

The summary of the results we found in this appendix is equations BOS1-BOS3 for bosons and FER1-FER3 for fermions.

Appendix B

Spectral Function

In this appendix we clarify the different Green's functions that were used in the text and give the relationships between them. We also introduce the spectral function which is crucial for passing from real frequency to imaginary time in Green's functions. What follows is largely based on Chapter 7 of [1].

At a manner similar to the imaginary time Green's functions which we introduced in Eq 2.18, we can define the real time Green's function as:

$$G(t) = -i \left\langle T \hat{X}_1(t) \hat{X}_2(0) \right\rangle \tag{B.1}$$

where the time ordering T works as in the imaginary time case and X_1, X_2 are arbitrary operators, which can be, for example, bosonic or fermionic creation/annihilation. We can think of these operators in the Heisenberg picture, where the time evolution is given by:

$$\hat{X}(t) = e^{it\hat{H}} \hat{X}(0) e^{-it\hat{H}} \tag{B.2}$$

It is also useful to define the retarded Green's function as:

$$G^R(t) = -i\Theta(t) \left\langle \left[\hat{X}_1(t), \hat{X}_2(0) \right]_p \right\rangle \tag{B.3}$$

where the index p in the commutator distinguishes the bosonic ($p = 1$) from the fermionic case ($p = -1$). For the latter the commutator becomes anticommutator.

We are interested in the real frequency Green's function which is the Fourier transform of Eq B.3. In order to show the calculation we expand the trace in the Hamiltonian

eigenbasis:

$$\left\langle \hat{X}_1(t)\hat{X}_2(0)\right\rangle = \frac{1}{\mathcal{Z}}\sum_{abcdf}\langle a|\, e^{it\hat{H}}\,|b\rangle\,\langle b|\,\hat{X}_1\,|c\rangle\,\langle c|\, e^{-it\hat{H}}\,|d\rangle\,\langle d|\,\hat{X}_2\,|f\rangle\,\langle f|\, e^{-\beta\hat{H}}\,|a\rangle =$$

$$= \sum_{ab} e^{it(\epsilon_a-\epsilon_b)-\beta\epsilon_a} X_{1ab}X_{2ba}$$

where $X_{iab} = \langle a|\,\hat{X}_i\,|b\rangle$ are the matrix elements and ϵ_i the Hamiltonian eigenvalues. This is known as the Lehmann representation. Hence we can write Eq B.3 as:

$$G^R(t) = -\frac{i\Theta(t)}{\mathcal{Z}}\sum_{ab} X_{1ab}X_{2ba}e^{it(\epsilon_a-\epsilon_b)}\left(e^{-\beta\epsilon_a} - pe^{-\beta\epsilon_b}\right) \tag{B.4}$$

The Fourier transform contains integrals like:

$$\int_{-\infty}^{+\infty} e^{i\omega t}\Theta(t)e^{it(\epsilon_a-\epsilon_b)}dt = \int_0^{+\infty} e^{it(\omega+\epsilon_a-\epsilon_b)}dt$$

To ensure convergence we add a factor $\eta\,|t|$, with $\eta \to 0^+$ to the exponential:

$$\int_0^{+\infty} e^{i(\omega+\epsilon_a-\epsilon_b)t-\eta t}dt = -\frac{1}{i(\omega+\epsilon_a-\epsilon_b)-\eta}$$

Hence Eq B.4 transforms to:

$$G^R(\omega) = \frac{1}{\mathcal{Z}}\sum_{ab} X_{1ab}X_{2ba}\frac{e^{-\beta\epsilon_a} - pe^{-\beta\epsilon_b}}{\omega+\epsilon_a-\epsilon_b+i\eta} \tag{B.5}$$

It is instructive to write the imaginary time and Matsubara frequency analog of Eqs B.4 and B.5.

$$G(\tau) = \left\langle \hat{X}_1(\tau)\hat{X}_2(0)\right\rangle = -\frac{1}{\mathcal{Z}}\sum_{ab} X_{1ab}X_{2ba}e^{(\epsilon_a-\epsilon_b)\tau-\beta\epsilon_a}\,, \quad \tau > 0 \tag{B.6}$$

$$G(\tau) = \left\langle \hat{X}_2(0)\hat{X}_1(\tau)\right\rangle = -\frac{1}{\mathcal{Z}}\sum_{ab} X_{1ab}X_{2ba}e^{(\epsilon_a-\epsilon_b)\tau-\beta\epsilon_b}\,, \quad \tau < 0 \tag{B.7}$$

If we substract B.6-B.7 and compute $G(\tau \to it+\eta) - G(\tau \to it-\eta)$ for $\eta \to 0^+$ we see that the result is identical to the retarded real time B.4:

$$G^R(t) = i\Theta(t)\left[G(\tau \to it+\eta) - G(\tau \to it-\eta)\right] \tag{B.8}$$

which gives the correct way to analytically continue the imaginary time function to find

the retarded. This is useful in Chapter 4 where we need the real time Green's functions to calculate the OTO correlator kernel.

Using the transformation of Eq 2.20, this gives:

$$G(i\omega_n) = -\frac{1}{\mathcal{Z}}\sum_{ab} X_{1ab}X_{2ba}e^{-\beta\epsilon_a}\int_0^\beta e^{(i\omega_n+\epsilon_a-\epsilon_b)\tau}d\tau \Rightarrow$$

$$\Rightarrow G(i\omega_n) = \frac{1}{\mathcal{Z}}\sum_{ab} X_{1ab}X_{2ba}\frac{e^{-\beta\epsilon_a} - pe^{-\beta\epsilon_b}}{i\omega_n + \epsilon_a - \epsilon_b} \tag{B.9}$$

We not that p here comes from $e^{i\omega_n\beta}$ which is 1 for bosons and -1 for fermions, as bosonic Matsubara frequencies are even multiples of π while fermionic are odd.

Comparing Eq B.9 with B.5, we see that the former can come from the latter by doing the transformation $i\omega_n \to \omega + i0^+$. This is known as the analytic continuation from Matsubara frequencies to real frequencies.

The spectral function can be defined as:

$$\rho(\omega) = -2\,\mathrm{Im}\,G^R(\omega) \tag{B.10}$$

We can find the corresponding Lehmann representation by taking the imaginary part of B.5. Notice that when $X_1 = X_2^\dagger$, as in the case of the bosonic/fermionic operators, the product $X_{1ab}X_{2ba}$ is real, so:

$$\rho(\omega) = -\frac{2}{\mathcal{Z}}\sum_{ab} X_{1ab}X_{2ba}\left(e^{-\beta\epsilon_a} - pe^{-\beta\epsilon_b}\right)\mathrm{Im}\,\frac{1}{\omega + \epsilon_a - \epsilon_b + i0^+} \Rightarrow$$

$$\Rightarrow \rho(\omega) = \frac{2\pi}{\mathcal{Z}}\sum_{ab} X_{1ab}X_{2ba}\left(e^{-\beta\epsilon_a} - pe^{-\beta\epsilon_b}\right)\delta(\omega + \epsilon_a - \epsilon_b) \tag{B.11}$$

because according to Dirac's identity:

$$\mathrm{Im}\lim_{\eta\to 0^+}\frac{1}{x+i\eta} = -\pi\delta(x)$$

The delta function in B.11 is the reason we can use the spectral function to go from a known real frequency $G^R(\omega)$ to the imaginary time $G(\tau)$, as in... . We introduce the delta function in B.6 as:

$$G(\tau) = -\int_{-\infty}^{+\infty}\frac{1}{\mathcal{Z}}\sum_{ab} X_{1ab}X_{2ba}e^{-\omega\tau-\beta\epsilon_a}\delta(\omega+\epsilon_a-\epsilon_b)d\omega =$$

$$= -\int_{-\infty}^{+\infty} \frac{1}{\mathcal{Z}} \sum_{ab} X_{1ab} X_{2ba} \left(e^{-\beta\epsilon_a} - p e^{-\beta\epsilon_b} \right) e^{-\omega\tau} \frac{\delta(\omega + \epsilon_a - \epsilon_b)}{1 - p e^{\beta(\epsilon_a - \epsilon_b)}} d\omega \Rightarrow$$

$$\Rightarrow G(\tau) = \int_{-\infty}^{+\infty} \frac{\rho(\omega)}{p e^{-\beta\omega} - 1} e^{-\omega\tau} \frac{d\omega}{2\pi} \tag{B.12}$$

which gives the relation between the real frequency Green's function (included in ρ) and the imaginary time. Following the same procedure for $\tau < 0$ we have:

$$G(\tau) = \int_{-\infty}^{+\infty} \frac{\rho(\omega)}{e^{\beta\omega} - p} e^{-\omega\tau} \frac{d\omega}{2\pi} \tag{B.13}$$

At a similar manner, spectral function can be used to connect the retarded real frequency function $G^R(\omega)$ with the Matsubara frequency function $G(i\omega)$. The result is obtained comparing B.11 with B.9 and it is:

$$G(i\omega_n) = \int_{-\infty}^{+\infty} \frac{\rho(\omega)}{i\omega_n - \omega} \frac{d\omega}{2\pi} \tag{B.14}$$

This result is known as the spectral representation and we can analytically continue it to complex plane $i\omega_n \to z \in \mathbb{C}$.

Appendix C

SD Equations Numerical Solution

Equations BOS1-BOS3 and FER1-FER3 are the main subject of Chapter 2, as every measurable quantity can be related to the Green's functions which solve these equations. In the main text we presented the $T = 0$ solutions in the infrared (small ω) as this is the only case where equations are easily solved. We also extended these solutions at finite temperature in the conformal limit $\beta J \ll 1$.

In the original work [2] and every subsequent paper, these analytic solutions are corroborated by a numerical solution of equations. Supplementary information of [10] provides an extensive explanation of the technique used to solve such equations and here we try to follow it.

The main idea is to start with a function that satisfies the low frequency behavior of the analytic solutions and goes to zero for $\omega \to \pm\infty$. Such a function can be of the form $G(\omega) \sim e^{-\omega^2}/\sqrt{\omega}$ in real frequencies. We can then calculate the corresponding self energy from FER2 written in real frequencies. Using FER1 in real frequencies we calculate the Green's function G_Σ that corresponds to this self energy. If G was a correct choice then it must be $G = G_\Sigma$, which means that G satisfies both equations. However, generally we have $G \neq G_\Sigma$ as we do not know the solution from the beginning. Hence, we use the rule:

$$G' = (1 - x)G + xG_\Sigma$$

proposed in [9], to update the Green's function and repeat the same steps. We start with $x = 0.5$ for the first update and then we track the difference $\sum |G - G_\Sigma|^2$. We compare this value with the previous step and if an increase is observed we reduce x to its half

value. The iteration ends when the difference becomes smaller than a specific value, which means that the solution converges satisfactorily.

The most technically difficult point of this algorithm is passing from G to Σ in real frequencies, as we need an analytic continuation of the Fourier transform of FER2. We use the equation derived in [10]:

$$\Sigma(\omega) = -i \int_0^{+\infty} \left[n_1^2(t) n_2(t) + n_3^2(t) n_4(t) \right] e^{i\omega t} dt$$

where

$$n_1(t) = \int_{-\infty}^{+\infty} \rho(\omega) n_{\mathrm{F}}(-\omega) e^{-i\omega t} d\omega \quad , \quad n_2(t) = \int_{-\infty}^{+\infty} \rho(\omega) n_{\mathrm{F}}(\omega) e^{i\omega t} d\omega$$

$$n_3(t) = \int_{-\infty}^{+\infty} \rho(\omega) n_{\mathrm{F}}(\omega) e^{-i\omega t} d\omega \quad , \quad n_4(t) = \int_{-\infty}^{+\infty} \rho(-\omega) n_{\mathrm{F}}(\omega) e^{-i\omega t} d\omega$$

where n_{F} is the Fermi-Dirac distribution (ω stands for energy since $\hbar = 1$). As proposed in the paper, these Fourier transform can be done numerically by discreticizing in frequencies and using a Fast Fourier Transform (FFT) algorithm. The main problem in our problem that does not exist in [10] (for $p > 0$) is the singularity at $\omega = 0$. This causes trouble in the calculation of $n_1, ..., n_4$ integrals. In order to solve this we use the fact that we know the exact form of the singularity from the low frequency behavior $\sim 1/\sqrt{\omega}$. We can write all these integrals in a form:

$$\int_0^{+\infty} \frac{F(\omega)}{\sqrt{\omega}} e^{-i\omega t} d\omega = \int_0^{+\infty} F(x^2) e^{-ix^2 t} dx$$

and absorb the singularity in dx by changing $x = \sqrt{\omega}$. Now we can calculate numerically this integrals by discretizing over $x^2 = \omega = mh$ with $m = 0, 1, ..., N-1$ and h an appropriate step. However, we must now notice that dx is different from step h but changes from point to point as $dx \approx \Delta x = \left(\sqrt{m+1} - \sqrt{m}\right)\sqrt{h}$. We might think that the singularity is hidden in this approximation. The integral can then be approximated by the sum:

$$\sum_{m=0}^{N-1} F_m e^{-imht} \left(\sqrt{m+1} - \sqrt{m}\right) \sqrt{h}$$

We wrote the program in Python, using the numpy package for mathematics. According to the documentation the FFT (and the corresponding inverse) commands calculate the

following sums:

$$A_k = \sum_{m=0}^{N-1} a_m \exp\left(-2\pi i \frac{mk}{N}\right) \quad , \quad a_m = \frac{1}{N}\sum_{k=0}^{N-1} A_k \exp\left(2\pi i \frac{mk}{N}\right)$$

Clearly the first sum is the same with the one we need. In order to make the exact correspondence we define the maximum frequency as $\omega_{\max} \equiv 2\pi M(1-1/N)$ where M is a value we set and it is

$$\omega_{\max} = (N-1)h \Rightarrow h = 2\pi\frac{M}{N}$$

The correspondence with the FFT sum gives $t = k/M$ therefore M actually sets the step for time (it is $1/M$). Since the total number of points in time is restricted to N, by changing the step $1/M$ we adjust how long we go in time. Therefore we may want to have long step (small M, for example $M \approx 2$) in order to go in long times. Integrals in time are calculated using the inverse FFT transform noticing that by default it carries an additional $1/N$.

We give the code for the fermionic case:

```
import numpy as np

def nF(b,x):
    return 1/(np.exp(b*x)+1)

class Green():
    def __init__(self,N,M):
        self.M=M
        self.N=N
        self.sqrtN=np.sqrt(N)
        self.w=np.linspace(0,2*np.pi*M*(1-1/N),N)
        self.sqrtw=np.sqrt(self.w)
        self.dw=np.sqrt(np.arange(1,N))-np.sqrt(np.arange(N-1))
        self.dw=np.append(self.dw,0)*np.sqrt(2*np.pi*M)
        L=np.sqrt(np.sqrt(np.pi)/2)*(1j-1)
        self.Fpos=L*np.exp(-self.w*self.w)
        self.Fneg=self.Fpos/1j
        self.dif=10000

    def calculate_newG(self,b):
        rhopos=-self.Fpos.imag/np.pi
        rhoneg=-self.Fneg.imag/np.pi
```

```
        n1=np.fft.fft(rhopos*nF(b,-self.w)*self.dw)/self.sqrtN
        n1+=np.fft.ifft(rhoneg*nF(b,self.w))*self.sqrtN
        n3=np.fft.fft(rhopos*nF(b,self.w)*self.dw)/self.sqrtN
        n3+=np.fft.ifft(rhoneg*nF(b,-self.w)*self.dw)*self.sqrtN
        Sw=-1j*self.N*np.fft.ifft(n1*n1*n1+n3*n3*n3)/self.M
        self.newFpos=-self.sqrtw/(self.w+Sw)
        Sw=-1j*np.fft.fft(n1*n1*n1+n3*n3*n3)/self.M
        self.newFneg=self.sqrtw/(self.w-Sw)

    def update(self,diflim,b,x):
        df=self.dif
        while df>diflim:
            print(df)
            self.calculate_newG(b)
            difv=np.append(np.absolute(self.newFneg-self.Fneg), &
                           np.absolute(self.newFpos-self.Fpos))
            df=sum(difv*difv)/self.N
            if df>self.dif:
                x*=0.5
            self.Fpos=(1-x)*self.Fpos+x*self.newFpos
            self.Fneg=(1-x)*self.Fneg+x*self.newFneg
            self.dif=df

F=Green(640000,2.2)
F.update(0.00001,1000,1)
```

Note: The reality is that this program does not work absolutely correct, meaning that the solution is not exactly this given in Figure 2.1. The solution found by the program becomes unstable at a small region around zero. This problem must be related to the singularity at this point, where a more fine lattice might be needed for the integrations. In order to get Figure 2.1 we erased the unstable points and rescaled the remaining function in order for the zero value to be the correct one.

Appendix D

Eigenvalue Equation Numerical Solution

In Chapter 4 we found the equation 4.28:

$$\tilde{f}(\omega) = \frac{k}{2}\left|\frac{\Gamma\left(m+i\omega\right)}{\Gamma\left(\frac{1}{2}+m+i\omega\right)}\right|^2 \int_{-\infty}^{+\infty} \frac{\tilde{f}(\omega')d\omega'}{\cosh\pi(\omega-\omega')} \tag{D.1}$$

where $m = (1+\mu)/2$ and $k = 1/2$ or $3/2$. Our goal is to find the values of m for which this equation has a solution $\tilde{f}(\omega)$. This can be done by treating this as an eigenvalue integral equations with kernel:

$$K(\omega,\omega') = \frac{k}{2}\left|\frac{\Gamma\left(m+i\omega\right)}{\Gamma\left(\frac{1}{2}+m+i\omega\right)}\right|^2 \operatorname{sech}\pi(\omega-\omega') \tag{D.2}$$

and finding the values of m for which K has eigenvalue 1. Finding eigenvalues of an integral operator analytically is generally not straightforward, but we can always take the discrete limit of the kernel and compute it numerically using the standard linear algebra procedure, treating D.1 as matrix multiplication $f_m = K_{mn}f_n$.

The problem is then reduced in calculating the matrix K_{mn}. This can be done easily in MATLAB using the Toeplitz[1] command. This command calculates the sech term of D.2, as this has a Toeplitz form. We also use P. Godfrey's algorithm to calculate Gamma functions, because MATLAB's Gamma function does not support complex arguments.

[1]Toeplitz matices are those of the form $A_{ij} = a_{i-j}$.

We find the eigenvalues of K matrix for different values of m and plot them in Figure 4.1. The code used is:

```
M=15;
N=200;
kappa=3/2;

Nm=300;
mv=linspace(0,1.6,Nm);

lv=zeros(5,Nm);
x=linspace(-M,M,N);

for j=1:Nm;
    m=mv(j);
    KER=toeplitz(-M-x);
    KER=1./cosh(pi*KER);
    F=kappa*abs(gammac(m+i*x)./gammac(0.5+m+i*x)).^2/2;
    F=ones(N,1)*F;
    KER=F.*KER;
    KER=KER*(x(2)-x(1));
    L=eig(KER);
    for k=1:5;
        lv(k,j)=L(k);
    end
end
```

Bibliography

[1] A. Altland and B. Simons. Condensed Matter Field Theory. *Cambridge University Press*, 2nd Edition, 2010.

[2] S. Sachdev and J. Ye. Gapless Spin-Fluid Ground State in a Random Quantum Heisenberg Magnet. *Physical Review Letters*, 70(21), May 1993.

[3] A. Georges, O. Parcollet, and S. Sachdev. Mean field theory of a quantum Heisenberg spin glass. *Physical Review Letters*, 85, 840, July 2000.

[4] A. Georges, O. Parcollet, and S. Sachdev. Quantum fluctuations of a nearly critical Heisenberg spin glass. *Phys. Rev. B*, 63, 134406, August 2001.

[5] L. Arrachea and M. J. Rozenberg. Mean field theory of a quantum Heisenberg spin glass. *Phys. Rev. B*, 65, 224430, June 2002.

[6] S. Sachdev. Bekenstein - Hawking entropy and strange metals. *Physical Review Letters*, arXiv:1506.05111, August 2015.

[7] A. Kitaev. Hidden correlations in the Hawking radiation and thermal noise. *KITP Theory Seminar*, February 2015.

[8] A. Kitaev. A simple model of quantum holography. *KITP Entagled15*, May 2015.

[9] J. Maldacena and D. Stanford. Comments on the Sachdev-Ye-Kitaev model. *Phys. Rev. D*, 94, 106002, November 2016.

[10] S. Benerjee and E. Altman. Solvable model for a dynamical quantum phase transition from fast to slow scrambling. arXiv:1610.04619 [cond-mat.str-el], 2016.

[11] P.W. Anderson. Theory of magnetic exchange interactions: exchange in insulators and semiconductors. *Solid State Physics*, 1963.

[12] M. Norman. Herbertsmithite and the search for the quantum spin liquid. *Rev. Mod. Phys*, 88, 041002, December 2016.

[13] G. Parisi M. Mezard and M. Virasoro. Spin Glass theory and beyond. *World Scientific Lecture Notes in Physics*, Volume 9, 1986.

[14] J. M. Maldacena. The large n limit of superconformal field theories and supergravity. *Adv. Theor. Math. Phys.*, 2:231–252, 1998.

[15] J. Maldacena, S. Shenker, and D. Stanford. A bound on chaos. *arXiv:1503.01409 [hep-th]*, May 2015.

[16] J. Polchinski and V. Rosenhaus. The spectrum in the Sachdev-Ye-Kitaev model. arXiv:1601.06768, 2016.

[17] E. Rozenbaum, S. Ganeshan, and V. Galitski. Lyapunov exponent and Out-of-Time-Ordered correlator growth rate in a chaotic system. *Phys. Rev. Lett.*, 118, 086801, February 2017.

[18] D. Stanford. Black holes and the butterfly effect. *Institute of Advanced Study - Ideas*, 2017.

[19] D. I. Pikulin and M. Franz. Black hole on a chip: proposal for a physical realization of the SYK model in a solid-state system. (arXiv:1702.04426 [cond-mat.dis-nn]), March 2017.

[20] A. J. Bray and. M. A Moore. Replica theory of quantum spin glasses. *Journal of Physics C Solid State Physics*, 13(24), June 1980.

[21] S. H. Strogatz. Nonlinear dynamics and chaos. *Perseus Books Publishing*, 1994.

[22] A. I. Larkin and Y. N. Ovchinnikov. Quasiclassical method in the theory of superconductivity. *Soviet Physics JETP*, June 1969.

[23] D. Roberts P. Hosur, X.-L. Qi and B. Yoshida. Chaos in quantum channels. *Journal of High Energy Physics*, February 2016.

[24] S. H. Shenker and D. Stanford. Black holes and the butterfly effect. *Journal of High Energy Physics*, March 2013.

[25] P. Hayden and J. Preskill. Black holes as mirrors: quantum information in random subsystems. *Journal of High Energy Physics*, September 2007.

[26] J. Maldacena. Black holes and the information paradox in string theory. *Institute of Advanced Study - Ideas*, 2011.

[27] I. L. Aleiner, L. Faoro, and L. B. Ioffe. Microscopic model of quantum butterfly effect: out-of-time-order correlators and traveling combustion waves. *Annals of Physics*, 375: 378–406, December 2016.